NUMERICAL INVESTIGATION OF POLYMER ADDITIVE EFFECTS ON THE FLOW AROUND IMMERSED BODIES

by

Onur Çetin

B.S., Mechanical Engineering, Boğaziçi University, 2009

Submitted to the Institute for Graduate Studies in
Science and Engineering in partial fulfillment of
the requirements for the degree of
Master of Science

Graduate Program in Mechanical Engineering
Boğaziçi University

2013

ACKNOWLEDGEMENTS

At first and foremost, I would like to thank my thesis supervisor Assoc. Prof. Kunt Atalık for all the encouragement, foresight and relieving guidance throughout my thesis study, providing a productive and cooperative atmosphere for research. I feel enormously lucky for being one of his students.

Then, I would like to express my thanks to the Scientific and Technological Research Council of Turkey (TUBITAK) for the financial assistance during the project coded 107M390.

I am also grateful to the members of my committee, Assoc. Prof. Ali Ecder and Assoc. Prof. Osman Börekçi, for their constructive comments and support.

Finally, I would like to express my endless thanks to my family and friends for their love, patience and support.

ABSTRACT

NUMERICAL INVESTIGATION OF POLYMER ADDITIVE EFFECTS ON THE FLOW AROUND IMMERSED BODIES

Although it is a well-known fact that dilute solutions obtained by adding a small amount of polymer or surfactant to Newtonian fluids lead to a reduction in friction factor and drag coefficient at high Reynolds number flows; its mechanism and the polymer induced flow structure at high Reynolds numbers need to be investigated in more detail for different flow geometries by means of new experimental methods, as well as numerical simulations with the application of different rheological constitutive models. For clarification of such an important part of fluid mechanics, numerical simulations have been performed with Newtonian, generalized Newtonian (Power-law) and viscoelastic (FENE-P) fluid models, Reynolds number up to 4000 for circular cylinder domain and Reynolds number up to 2000 for square cylinder domain. The results of the simulations have been compared with literature. The most distinctive consequences of these simulations is that Power-law fluid, not the viscoelastic fluid, causes decrease in drag coefficient and increase in vortex shedding frequency in the wake region compared to Newtonian fluid, for both circular and square cylinder simulations. It is also concluded that polymer addition, with respect to Power-law fluid, results in an opposite effect, on vortex formation length and drag coefficient, at high Reynolds numbers.

ÖZET

CİSİM ETRAFI AKIŞLARDA POLİMER KATKISININ AKIŞ YAPISINA ETKİSİNİN SAYISAL OLARAK İNCELENMESİ

Newtonyen akışkanlara az miktarda polimer veya sürfaktant eklenmesiyle elde edilen seyreltik çözeltilerin yüksek Reynolds sayılarındaki akışlarında sürtünme faktörü ve sürükleme kuvvetinde indirgeme gözlendiği uzun süredir bilinen bir konu olmasına rağmen bu etkiye yol açan mekanizma ve bu etkinin yüksek Reynolds sayılarında akış yapıları üzerindeki sonuçlarının çeşitli akış geometrilerinde yeni deneysel yöntemler ve reolojik bünye modelleri uygulayarak daha ayrıntılı irdelenebilmesi yönünde çalışmalara ihtiyaç vardır. Akışkanlar mekaniğinin bu önemli noktasının açığa kavuşturulması için; bu çalışmada numerik simulasyonlar Newtonyen, genelleştirilmiş Newtonyen (Power-law modeli) ve viskoelastik (FENE-P) akışkan modelleriyle yuvarlak silindir üzeri Reynolds sayısı 4000'e kadar ve kare silindir üzeri Reynolds sayısı 2000'e kadar olan koşullarda yürütülmüştür. Simulasyonların sonuçları literatürle karşılaştırılarak tutarlı olup olmadıkları anlaşılmaya çalışılmıştır. Simulasyonların en belirgin sonucu da, Power-law akışkanının Newtonyen akışkana göre yuvarlak ve kare silindir üzeri akışlarda sürükleme katsayısında azalma ve girdap oluşum frekansında artmaya yol açması olmuştur. Ayrıca, polymer katkısı, Power-law modeline göre, yüksek Reynolds sayılarında sürükleme katsayısı ve vortex oluşum uzaklığına tam ters etki yaratmaktadır.

TABLE OF CONTENTS

LIST OF FIGURES

LIST OF TABLES

LIST OF SYMBOLS

A	FENE-P configuration tensor
C_d	Drag coefficient
d	Cylinder diameter / Characteristic length
D	Rate of deformation tensor
D/Dt	Material derivative
$\vec{F}_{cv}$	Acting forces on the control volume
$\vec{g}$	Gravity vector
I	Identity tensor
k	Turbulence kinetic energy
l	Vortex formation length
$\vec{L}$	Linear momentum vector
L	Polymer chain length
m	Power-law consistency factor
M	Mass
n	Power-law index
p	Pressure
Re	Reynolds number
St	Strouhal number
T	Stress tensor / Total extra stress tensor
T_1	Viscoelastic stress tensor
T_2	Newtonian stress tensor
$\vec{u}$	Velocity vector
$\vec{U}$	Local mean velocity
v_i	Lateral component of velocity at a time step
$\vec{V}$	Free stream velocity
We	Weissenberg number

β	Viscosity ratio
$\dot{\gamma}$	Shear rate
λ	Relaxation time
η	Viscosity
ρ	Density

LIST OF ACRONYMS / ABBREVIATIONS

CFD	Computational Fluid Dynamics
DNS	Direct Numerical Solutions
FENE-P	Finitely extensible nonlinear elastic – Peterlin
PIV	Particle Image Velocimetry
RMS	Root Mean Square

1. INTRODUCTION

1.1. Background

The problem of a body immersed in a moving fluid has been one of the main problems in fluid mechanics. Up to now, many studies have been performed related to this problem due to its direct applications in several engineering fields including flow around airplanes, automobiles, heat exchangers, tall buildings, bridges, etc. Flow around circular and square cylinders is investigated both theoretically and numerically, in order to simplify these real life problems. This simplification is required because setting up, investigating and solving a problem is getting much easier both experimentally and numerically with a simplified geometry instead of a much more complicated real geometry.

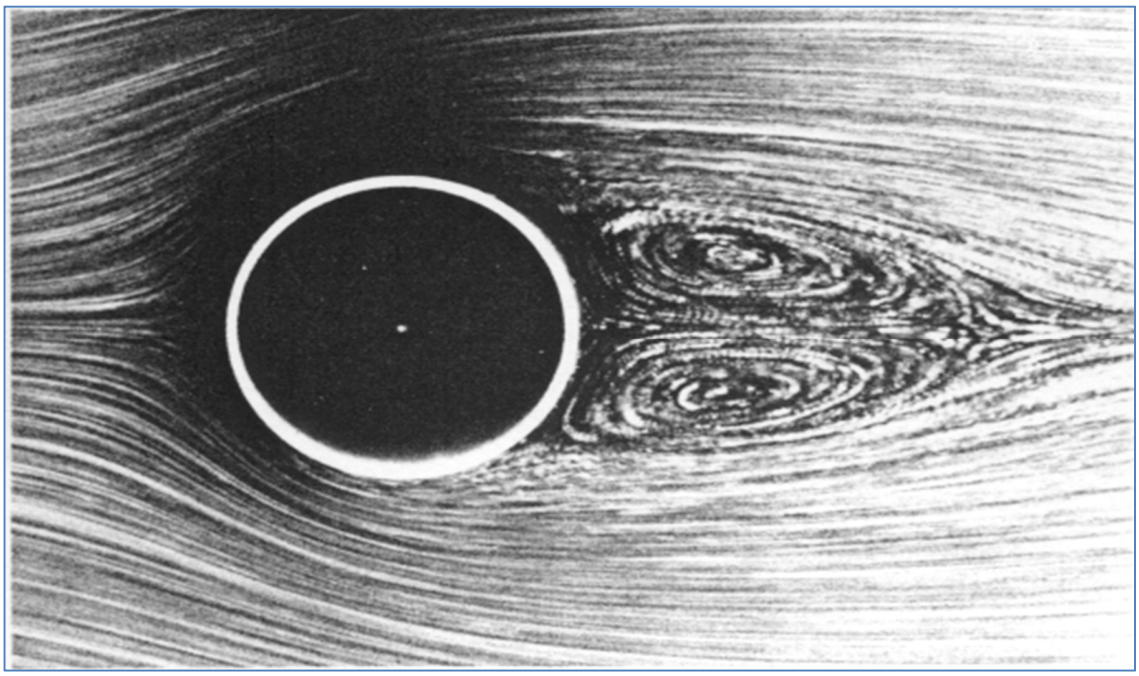

Figure 1.1. An illustration of the flow around circular cylinder [1].

It is well known for the last 50 years that obtaining dilute polymer solutions by adding just a few parts per million (ppm) of polymer or surfactant to Newtonian fluids affects the characteristics of the flow significantly. It is also observed that the effect of polymer addition

on the flow characteristics leads to a reduction in friction factor, loss of momentum and drag coefficient at high Reynolds numbers so that this effect is used in many external and internal flow applications like fluid transport systems [2], some medical applications [3], and flow around torpedoes [4]. In fact, the most remarkable economical return of this flow characteristic change has been the use of polymers in the trans-Alaska pipeline system; this resulted in a flow rate increase of 32,000 m^3 per day, where the downstream injected oil-soluble polymer concentration is about 10 ppm [5]. A similar application is the addition of polymers to the pumped oil from offshore platforms to shore facilities. Reducing the drag by ejecting a polymer and sea-water solution through torpedo nose is another possibility, which is patented as a military application [6]. Moreover, in order to increase the flow rates in sewerage pipes and storm-water drains, polymers solutions have been used, so that the peak loads could not cause overflowing; if only relatively infrequent use is required, this has to be much cheaper than building new pipes [7]. In spite of all these well-known facts, the physical mechanism of flow characteristics change due to polymer addition is still not completely clear, neither with respect to polymer concentration nor Reynolds number range; hence it is still under investigation.

Apart from such practical applications, from a fundamental fluid dynamics point of view, the drag can be reduced by up to 70 percent by adding just a small amount (100 ppm) of long-chain polymer molecules in pipe flows [8]. The first studies on polymer induced flows have been done in 1949 by Toms [9] and Mysels [10], especially on turbulent straight pipe flows. There are also some early studies on the effect on flow around immersed bodies. For instance, in 1966, Gadd has shown that the vortex street in the immersed body wake region is affected by polymer addition [11]. It has also been shown by Kudin and Kalashnikov, in 1970s, that vortex shedding frequency is smaller for polymer added flows compared to the Newtonian ones without polymer addition [12]. In parallel, Sarpkaya *et al*. [13] have conducted a detailed analysis on flow separation and turbulence under polymer addition, and concluded that these flow characteristics are delayed by the use of polymer additives.

Cadot and Kumar indicated that fluid elasticity is the main reason for the decrease in vortex shedding frequency, or the increase in the vortex formation length with increasing

Reynolds number [14]. Similarly, Oliveira's study has shown the increase in vortex formation length and decrease in Strouhal number, which is non-dimensional indicator of vortex shedding frequency, is due to fluid elasticity between Re = 50 and Re = 140 [15]. However, more recently, it has been experimentally verified by Coelho and Pinho that vortex shedding frequency is directly proportional to polymer concentration, i.e. non-Newtonian fluids have higher Strouhal number than Newtonian fluids [16]. The reason for this contradiction may be the fact that the shear thinning properties of the fluid causes a decrease in boundary layer thickness in laminar flow which in turn increases the diffusion length and therefore the vortex shedding frequency.

As the effect on drag coefficient by polymer additives is taken into consideration; Tabor and de Gennes theorizes that it is the elastic behavior of the polymer chains that prevents the production of turbulent fluctuations at small scales so that increase in polymer concentration results in drag reduction [17]. On the other hand, Lumley proposed that stretching of the polymers in the buffer layer region increases the effective viscosity of the solution, thus leading to a thickening of the viscous sub-layer and, as a consequence, to the drag reduction [18]. In parallel, Den Toonder has shown, in 1997 and 2005, that polymer additives create the drag reduction, where viscous anisotropic stresses introduced by extended polymer is the main reason for the drag reduction whereas elasticity has adverse effect on drag reduction [19, 20]. In 1998, Dimitropoulos and Beris have found out in their study that polymer additives create drag reduction, where polymer extensional viscosity plays a significant role [21]. On the other hand, Ogata *et al*. [22] has investigated experimentally on surfactant solutions and noted that drag coefficient increases compared to that in tap water in the lower Reynolds number range whereas the drag coefficient decreases in the higher Reynolds number range. More specifically, drag coefficient of a cylinder with 20 mm diameter increases compared to that of Newtonian case in $1000 < Re < 3000$ range whereas it reduces at $3000 < Re < 10000$, and maximum drag reduction occurs at Re = 7000 up to 55% for 200 ppm surfactant solution. The main reason for drag increase at lower Reynolds number is the existence of a wide stagnation zone around cylinder and increasing shear viscosity.

More recently, Xiong *et al*. has numerically found out in their studies about flow around circular cylinders, in 2010 [23], that drag reduction is proportional with vortex formation

length. Their numerical results also show that the drag on a circular cylinder can be enhanced for low Reynolds numbers but can be reduced for higher ones due to the fact that polymer can make the wake region stable and unstable again for high Reynolds numbers. Also, Xiong *et al*. [24] have verified in 2011, that the drag reduces with increasing Weissenberg number for high Reynolds number polymer solutions till drag reduction reaches its maximum point, which is around 50% drag reduction; and after that point, increasing Weissenberg number has an adverse effect that creates drag enhancement.

Although there is lack of literature background in terms of polymer additive effects on the flow around square or rectangular cylinders, there have been Newtonian flow studies with square and rectangular cylinders, in order to simulate air and water flow around blunt bodies such as buildings, bridges, and ship structures. Bearman's [25] and Durao's [26] studies in 1980s are the initial studies about the flow around square cylinders. For instance, a more recent study by Luo *et al*. [27], which is about aero-elastic flow instability that is created by galloping oscillation of a square cylinder, has increased the interest in flow around square cylinders. Moreover, it needs to be taken into account, in flow around square cylinder studies, that the separation point is an invariable point, different from the circular cylinder flows, due to geometric properties. Dutta *et al*. [28] has shown the effect of separation point difference on wake region characteristics.

1.2. Rheology

Although many years of research have been devoted to the study of fluids of low molecular weight, which are described by Navier-Stokes equations, many challenging problems in both theory and applications remain. But, even more challenging are non-Newtonian fluids, whose motion cannot be described only by the Navier-Stokes equations. In order to understand, investigate and evolve this side of the fluid mechanics, i.e. non-Newtonian fluid mechanics, each scientist or engineer has put a milestone for the development of rheology. Rheology is the branch of science which studies the deformation and flow of matter, especially non-Newtonian flow of liquids and plastic flow of solids.

Air and water can be given as the most well-known examples of Newtonian fluids whereas plastics manufacture, performance of lubricants, application of paints, foodstuffs processing, movements of biological fluids, polymer solutions, molten polymers, and liquid crystals are the examples of non-Newtonian fluids applications. Compared to the Newtonian ones, non-Newtonian fluids can show quite strange and unexpected flow behaviour completely different than that of water or air, as described by Bird *et al*. [29]. For instance, drag reduction is one, and the most important, of these unexpected and counter-intuitive effects.

Non-Newtonian fluids can be described as the fluids that cannot be classified within the constitutive relation of Newton, in which the stress is linearly proportional to the deformation rate. In other words, the shearing stress is linearly related to the rate of shearing strain for Newtonian fluids whereas the shearing stress is not linearly related to the rate of shearing strain for non-Newtonian fluids. In more detail, as shown in Figure 1.2, the non-Newtonian fluid shows a shear thinning fluid behaviour if its viscosity decreases with increasing shear rate; on the contrary, it shows a shear thickening fluid behaviour if its viscosity increases with increasing shear-rate. Colloidal suspensions and polymer solutions are the examples of shear thinning fluids whereas water-cornstarch mixture and water-sand mixture are examples of shear thickening fluids. Besides, the other type of fluid behaviour shown in Figure 1.2, in terms of shear rate dependency, is the Bingham plastic. It symbolizes a material, neither a fluid nor a solid, that can withstand a finite shear stress without motion like a solid; but once its yield stress is exceeded, it flows like a fluid. Toothpaste and mayonnaise are common examples of Bingham plastic materials [29, 30].

In order to simulate the shear-rate dependent fluid viscosity models, where the viscosity is not constant, there are several Generalized Newtonian models developed; such as Power-law, Bird-Carreau law, Cross law, Bingham law. Power-law model is the most known and commonly used Generalized Newtonian model in the literature.

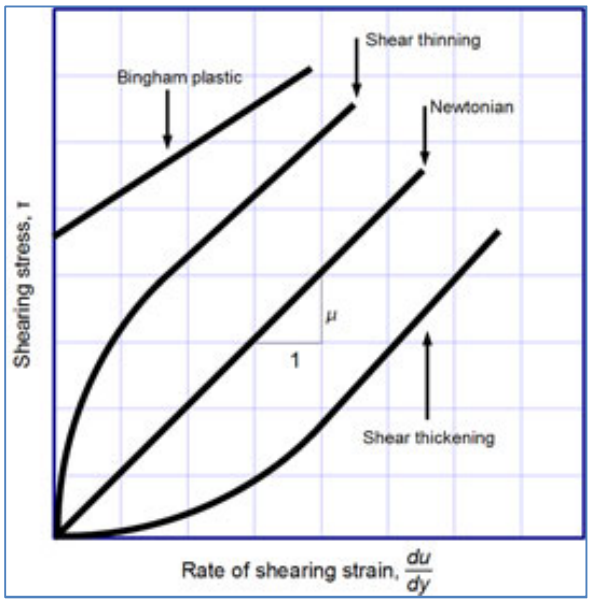

Figure 1.2. Variation of shearing stress with the rate of shearing strain for several types of fluids [30].

Apart from the inelastic fluid models listed above, there are also viscoelastic models, represent the materials that exhibit properties of both fluid behavior (viscous) and solid behavior (elastic). Viscoelastic materials show properties of both types of materials. When the applied stress on a viscoelastic material is removed; the effect of the stress does not vanish directly. Internal structure of the material maintains the stress for some time, this is called as fluid memory and this time period is called as relaxation time, which is a material dependent property. Thus, it can be stated that the relationship between stress and strain is time-dependent for viscoelastic materials, and fluids [31].

The main approach on the viscoelastic constitutive models is that the polymer induced fluid is represented by a purely viscous damper and a purely elastic spring connected to each other; and the stress tensor is decomposed into purely viscous and viscoelastic stress components. In the simplest of terms, when a constant stress is applied to a viscoelastic fluid, the strain has two components; elastic and purely viscous. Elastic component of the strain occurs instantaneously, corresponding to the spring, and relaxes immediately after release of the stress. The other component, the viscous component, grows with time as long as the stress

is applied. Maxwell, Oldroyd-B, Phan-Thien-Tanner, Giesekus, FENE-P (Finitely Extensible Nonlinear Elastic – Peterlin) are the most known viscoelastic constitutive models [32]. The FENE-P viscoelastic model is the most commonly used polymer model, used in turbulence simulations.

1.3. Turbulence

Fluid flow can be divided into three, with respect to flow manners; laminar, turbulent and transition. Laminar flow represents low fluid velocities, smooth sliding of adjacent layers, as well as constant velocity vector fields. On the other hand, turbulent flow symbolizes curling of field lines, mixing between adjacent layers and flow patterns increasingly turbulent towards high velocities. The third type of flow manner is the transition from laminar to turbulent flow. Basically, these three types of flow behaviour are distinguished from each other by means of a dimensionless parameter, Reynolds number, which is the ratio between inertial effects and viscous effects. For instance, flow in a circular pipe is laminar if Reynolds number is less than approximately 2100, and it is turbulent if Reynolds number is greater than approximately 4000; the Reynolds number range in between 2100 and 4000 is the transition. On the other hand; for most external flows, as a rule of thumb, flows with $Re < 1$ are dominated by viscous effects whereas flows with $Re>100$ are dominated by inertial effect [30].

In more detail, the turbulent flow is a flow regime which stands for a fluctuating and chaotic state of fluid motion where non-linear inertial effects dominate over viscous effects. Due to such instabilities and non-linear governing equations of turbulent flow, a complete theory of turbulence still lacks in fluid dynamics. This is why turbulence problems are always treated statistically rather than deterministically.

Although it has been accepted in the literature that drag coefficient is inversely proportional with Reynolds number since viscous forces become negligible compared to inertia forces with increasing Reynolds number; generated vortices and instabilities in turbulent flow numbers has an increasing effect on the drag coefficient [33]. This ambiguous

point is one of the reasons for the researchers that make the turbulence interesting. Thus, there are lots of studies, both theoretical and practical, to explore and develop turbulent drag reduction; such as polymer or surfactant addition into the flow, as explained previously. Micro bubbles injection, air films injection, electromagnetic turbulence control, rigid fiber addition, and using sinusoidal riblets are some of the other ideas emerged for turbulence drag reduction [34, 35, 36].

Figure 1.3. An example of turbulent flow in an airplane wake region [37].

Unfortunately, there is no universal theory of turbulence emerged for the solution of turbulence problems in spite of a concerted effort by engineers, physicists, and mathematicians since decades. Numerous experimental methods and numerical techniques have been developed for turbulent flow solution due to lack of an analytical solution of turbulence. One of the well-known experimental methods is Particle Image Velocimetry (PIV), which is an optical technique that opens the possibility to study the coherent structures quantitatively [38]; whereas Direct Numerical Solution (DNS) is one of the numerical techniques, which is based on solving the governing equations that describe the spatial and temporal evolutions of flows numerically, without any approximation for the turbulence. Giving the information which is very difficult to obtain in the laboratory is the major advantage of DNS compared to

laboratory experiments. However, DNS is also restricted to the simple geometries, low Reynolds numbers and Newtonian fluids, due to the need of high computational power to perform DNS [39].

Due to unpredictable behaviour of turbulence, time averaged forms of governing equations are generally used and semi-empirical mathematical models are introduced for turbulence modeling. The main categories of turbulence modeling are; algebraic (zero-equation), one-equation, two-equation, and second-order closure models.

Algebraic (zero-equation) models generally use an eddy viscosity approach to calculate the Reynolds stress; whereas one-equation models have been developed, as an alternative to algebraic models, to improve turbulent flow predictions by solving one additional transport equation. In one-equation models, solving for the characteristic velocity scale, which is proportional to the root square root of the specific kinetic energy of turbulence fluctuations, is the most popular method. This characteristic quantity is generally referred to the turbulence kinetic energy and it is denoted as, k.

Two-equation models, such as $k - \varepsilon$ and $k - \omega$ models, are the most commonly used turbulence models for a wide range of engineering work; and they provide independent transport equations for both turbulence length scale and the turbulence kinetic energy. The second-order closure models, which do not share the same wide use as the more popular two-equation or algebraic models due to their increased complexity, solve for the Reynolds stresses by means of partial differential equations [40].

1.4. Aim of the Thesis

Since the effect of polymer (or surfactant) addition on turbulent flow is not clarified, due to being an intersection point of two unsolved classical mechanics problems as turbulence and rheology, in detail yet; studying polymer induced turbulent flow has a significant worth in

terms of fluid mechanics. This investigation also intends to understand Newtonian turbulent flows, as well as non-Newtonian turbulence flows.

As mentioned, there is a significant gap especially in polymer induced external flow literature, due to the fact that most of the studies are based on internal flow. New experimental methods and advances in rheological constitutive modeling are needed in order to put the literature about the effects of polymer addition on flow characteristics on a reliable basis. Hence, this master thesis aims understanding and explanation of this fluid mechanics problem. Numerical methods are applied since they offer a better opportunity to analyze more complicated problems where it is hard to conduct experimental studies.

1.5. Scope of the Thesis

In order to help on putting the existing knowledge and experience of polymer induced turbulent flow into a reliable basis, as mentioned in previous section, simulations of Newtonian, Generalized Newtonian Power-law model, and viscoelastic FENE-P model have been performed for the flow around circular and square cylinders, with 10 mm characteristic dimension, in this master thesis. The Reynolds number range varies from 200; up to 4000 for the circular simulations, and up to 2000 for the square simulations.

The plan of the remainder of this thesis is to explain all these studies and compare with the literature as follows; Chapter 2, Problem Statement, defines the problem by explaining the geometry, domain, governing models and governing equations. Chapter 3, Numerical Methods and Calculations, mostly explains the computational part of the study, mesh-generation, mesh independency, and definition of problem input parameters. Chapter 4, Results and Discussions, shows simulations results in terms of drag reduction, vortex formation length, wake region velocity profiles, vortex shedding frequency, by comparing with the literature. Finally, Chapter 5, Conclusion, indicates the final outcome of the study by evaluating the result parameters.

2. PROBLEM STATEMENT

2.1. Domain and Geometry

For the investigation of the effect of polymer addition on flow around immersed bodies, the problem needs to be simplified for a better understanding and analysis. So, as seen in most of the numerical studies, imagining a two-dimensional relatively infinite domain with a circle in the middle instead of solving the problem in a three-dimensional real domain also helps for faster solution. As shown in Figure 2.1, the circle, which represents cross section of a circular cylinder, is located on the slightly left hand side of the middle of the two dimensional domain. This is because of the fact that the incoming flow comes from the left hand side of the cylinder and passes through it, and the right hand side of the cylinder will be investigated as wake region, which is significant in terms of post-processing section. In other words, setting the wake region larger, compared to the front zone, of the external flow is an advantage for the analysis of the problem.

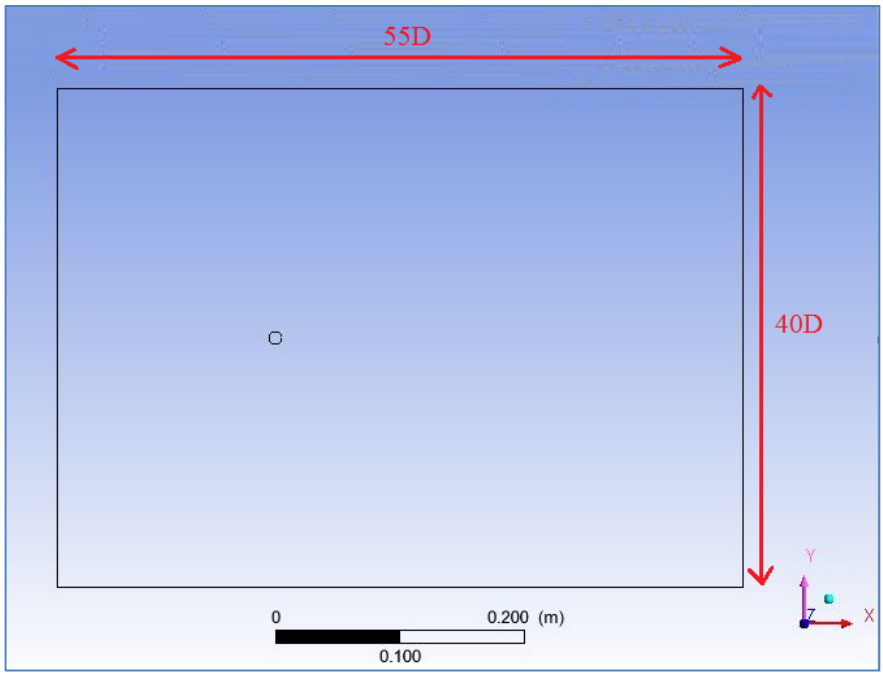

Figure 2.1. Two dimensional domain of the circular cylinder problem.

Figure 2.1 shows that the aspect ratios of the circular cylinder domain are 55 and 40 cylinder diameters, respectively; i.e. the width is 550 mm and the domain height is 400 mm while the cylinder diameter is 10 mm. The selected aspect ratios are also reasonable values considering previous studies. On the other hand, as shown in Figure 2.2 square cylinder domain has aspect ratios of 45 and 20 cylinder diameters; i.e. 450 mm width, 200 mm height, and 10 mm square sides; in parallel with the literature [41, 42].

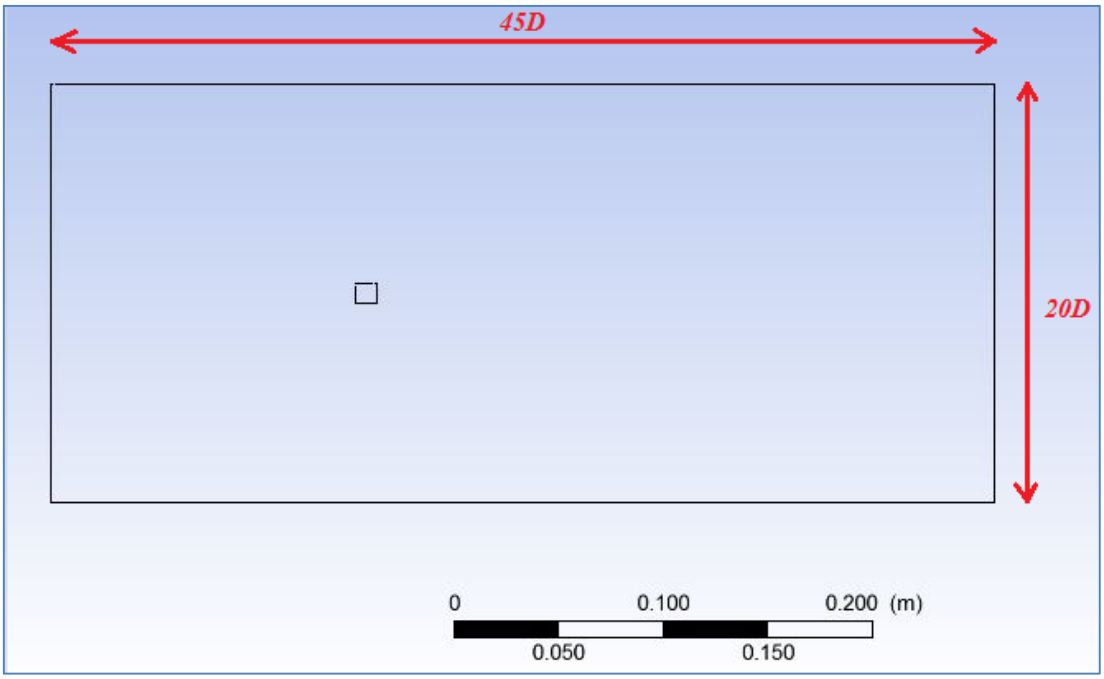

Figure 2.2. Two dimensional domain of the square cylinder problem.

2.2. Basic Equations

After determining the domain and geometry of the problem, the next step is defining the basic equations. The main equations of the problem, with incompressible two-dimensional flow assumption, are continuity equation (Equation 2.1) and linear momentum equation (Equation 2.2).

$$\frac{DM}{Dt} = 0 \rightarrow \frac{\partial \rho}{\partial t} + \nabla \cdot (\rho \vec{u}) = 0 \rightarrow \nabla \cdot \vec{u} = 0 \qquad (2.1)$$

where D/Dt is material derivative, M is mass, ρ is density, $\vec{u}$ is velocity vector.

$$\frac{D\vec{L}}{Dt} = \sum \vec{F}_{cv} \qquad \rightarrow \quad \rho \frac{D\vec{u}}{Dt} = \rho\vec{g} + \nabla \cdot T \tag{2.2}$$

where $\vec{L}$ is linear momentum vector, $\vec{g}$ is gravity vector, $\vec{F}_{cv}$ represents acting forces on the control volume and T is the stress tensor. T can be written, in Newtonian case, as:

$$T = -pI + 2\eta D \tag{2.3}$$

where p is the pressure, I is the identity tensor, η is the viscosity, D is the rate of deformation tensor for incompressible flow case. The momentum equation becomes:

$$\rho \frac{D\vec{u}}{Dt} = \rho\vec{g} + \nabla p + \eta\nabla^2\vec{u} \tag{2.4}$$

In Power-law, or a Generalized Newtonian model, where the viscosity of the fluid is considered as a function of the shear rate, is modeled using the following relation:

$$\eta(\dot{\gamma}) = m\dot{\gamma}^{n-1} \tag{2.5}$$

where $\dot{\gamma}$ is the shear rate, m is the consistency factor, and n is the power-law index. When n equals to 1, the model represents the Newtonian fluid; when n is less than 1, the fluid is shear thinning; and when n is greater than 1, the fluid is shear thickening. Then, the stress tensor T in the Navier-Stokes equations becomes:

$$T = -pI + 2\eta(\dot{\gamma}) = -pI + m\dot{\gamma}^{n-1}D \tag{2.6}$$

FENE-P model, which is a differential viscoelastic model based on molecular theories using dumbbell representation for infinitely extensible polymer chain, predicts a realistic shear

thinning of the fluid. The total stress tensor in momentum equation is decomposed into three components in the FENE-P model, as follows:

$$T = -pI + T_1 + S \tag{2.7}$$

where T_1 is purely-viscous component of the total stress tensor, and S is the viscoelastic component of the total stress tensor:

Purely-viscous stress tensor, T_1 can be written as:

$$T_1 = 2\,\eta_1 D \tag{2.8}$$

where η_1 is the viscosity coefficient for the purely-viscous component of the stress tensor.
The viscosity ratio β is defined as:

$$\beta = \frac{\eta_1}{\eta} \tag{2.9}$$

where η stands for the total viscosity.
Then, the purely-viscous and viscoelastic components of the total viscosity can be denoted as:

$$\eta_1 = \beta\eta \tag{2.10}$$

and

$$\eta_2 = (1-\beta)\,\eta \tag{2.11}$$

the viscoelastic component of the stress tensor S is defined as:

$$S = \frac{\eta_2}{\lambda}\left[\frac{A}{1-\frac{A}{3L^2}} - \frac{I}{1-\frac{I}{L^2}}\right] \tag{2.12}$$

where A, configuration tensor (state variable) is computed from the following differential equation:

$$\frac{A}{1-\frac{A}{3L^2}} + \lambda \overset{\nabla}{A} = \frac{I}{1-\frac{I}{L^2}} \tag{2.13}$$

$$\overset{\nabla}{A} = \frac{DA}{Dt} - \nabla u^T \cdot A - A \cdot \nabla u \tag{2.14}$$

where the operator $(\overset{\nabla}{\ })$ denotes the upper convected derivative, and $\overset{\nabla}{A}$ is the upper convected derivative of the configuration tensor A, ∇u is the velocity gradient, ∇u^T is the transpose of the velocity gradient, L is polymer chain length (the ratio of maximum length of a spring or, the polymer chain, to its length at rest); and λ is the relaxation time, which is a measure of the time required for the energy stored in the spring to dissipate [29, 43].

Varying polymer chain length represents the differentiation of polymer type. On the other hand, increasing relaxation time is proportional with increasing polymer concentration or increasing elasticity. The dimensionless parameter Weissenberg number, *We*, is defined as;

$$We = \frac{\lambda V}{d} \tag{2.15}$$

where V is the free stream velocity, and d is the characteristic length.

The Reynolds number, which is the ratio of inertia forces to the viscous forces, is defined as;

$$Re = \frac{\rho V d}{\eta} \tag{2.16}$$

Strouhal number, the non-dimensional indicator of vortex shedding frequency; is named after a Czech physicist Vincenc Strouhal who experimented in 1878 with wires experiencing vortex shedding and singing in the wind. It can be shown as:

$$St = \frac{f\,d}{V} \tag{2.17}$$

where *f* is the vortex shedding frequency [14].

Vortex formation length indicates the distance between the cylinder and the point with zero velocity at the centerline of the cylinder in the stream-wise direction. Although, the starting point of vortex formation length changes from study to study in the literature (the center of the cylinder or the end point of the cylinder); in this study, the vortex formation length *l* is defined as shown in Figure 2.3 [44].

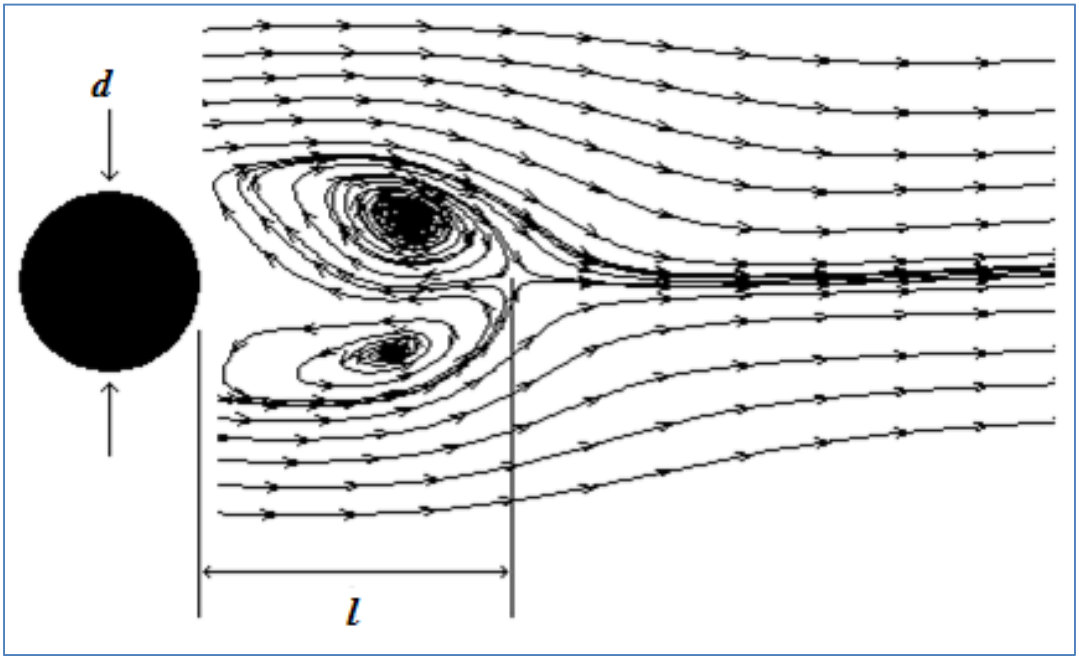

Figure 2.3. Definition of vortex formation length [44].

3. NUMERICAL METHODS AND CALCULATIONS

As mentioned in the previous section, numerical methods are required to solve the problem of polymer induced flow around cylinders since the governing equations cannot be solved with analytical methods. Thus, in this section, methods of computational fluid dynamics (CFD); which evolves replacing the partial differential equations with discretized algebraic equations that approximate the partial differential equations; are shown, step by step, in order to explain the problem solution in more detail.

3.1. Mesh Generation

The cylinder, either circular or square, is considered to be infinitely long and the aspect ratio is large enough to assume a two-dimensional flow field instead of a three-dimensional flow field. The two-dimensional problem solution takes much less computer time due to simplification of the problem. The computational mesh is generated using the mesh modeling program Gambit. Then, the finite element method is applied for the problem solution.

3.1.1. Mesh Generation for Circular Cylinder Problem

After creating the geometry in Gambit, the next step is mesh generation inside the defined geometry by considering the fact that the denser mesh is much better around the cylinder, especially in the wake region. As the distance from the cylinder increases, the mesh elements get larger in order to solve the problem. The last step is the definition of the boundaries of the domain such as inflow, outflow, and edge boundary conditions. Inflow and outflow boundary conditions are for incoming and outgoing flow whereas edge boundary conditions mean zero force boundary conditions at the edges.

Figure 3.1 shows one of meshes, which contains 16012 elements, with 10 mm circular cylinder diameter, and 550 mm to 400 mm rectangular domain dimensions.

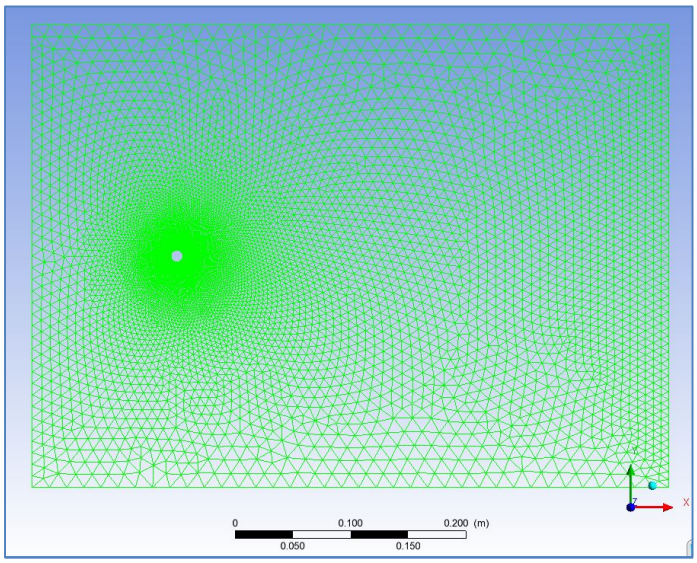

Figure 3.1. Mesh created in Gambit (Mesh A) for circular cylinder problem.

In circular cylinder case, there are several meshes generated for the above explained geometry. But, only three of them are used in the simulations by means of mesh independency check. The first one of the three meshes, which can be called as Mesh A, as shown in Figure 3.1, is the coarser mesh whereas the second one, Mesh B, shown in Figure 3.2, is a finer mesh with 32116 elements; and mesh C with 36458 elements is the last one.

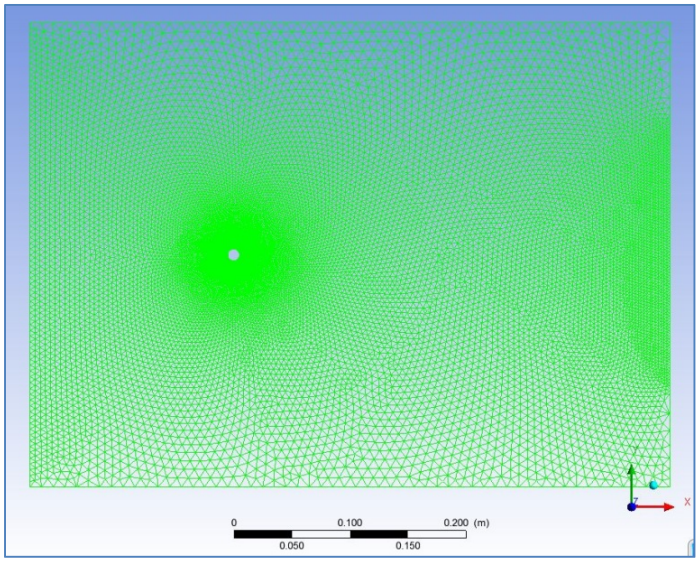

Figure 3.2. Mesh created in Gambit (Mesh B) for circular cylinder problem.

3.1.2. Mesh Generation for Square Cylinder Problem

Similar to the circular cylinder case, a two dimensional rectangular domain is defined by locating a square in the middle, to represent the square cylinder. The rectangular domain has the dimensions of 450 mm and 200 mm, while the edge of the square is set as 10 mm in parallel with the circular cylinder diameter dimension as a characteristic length parameter. The boundary conditions are defined similar to the circular cylinder case; as inflow, outflow, and edge boundary conditions.

Two different meshes have been used in square cylinder simulations. The first one, which is called as Mesh X, contains 57536 mesh elements; and the second one, called as Mesh Y, contains 89900 mesh elements. Mesh X and Mesh Y are shown in Figures 3.3 and 3.4, respectively.

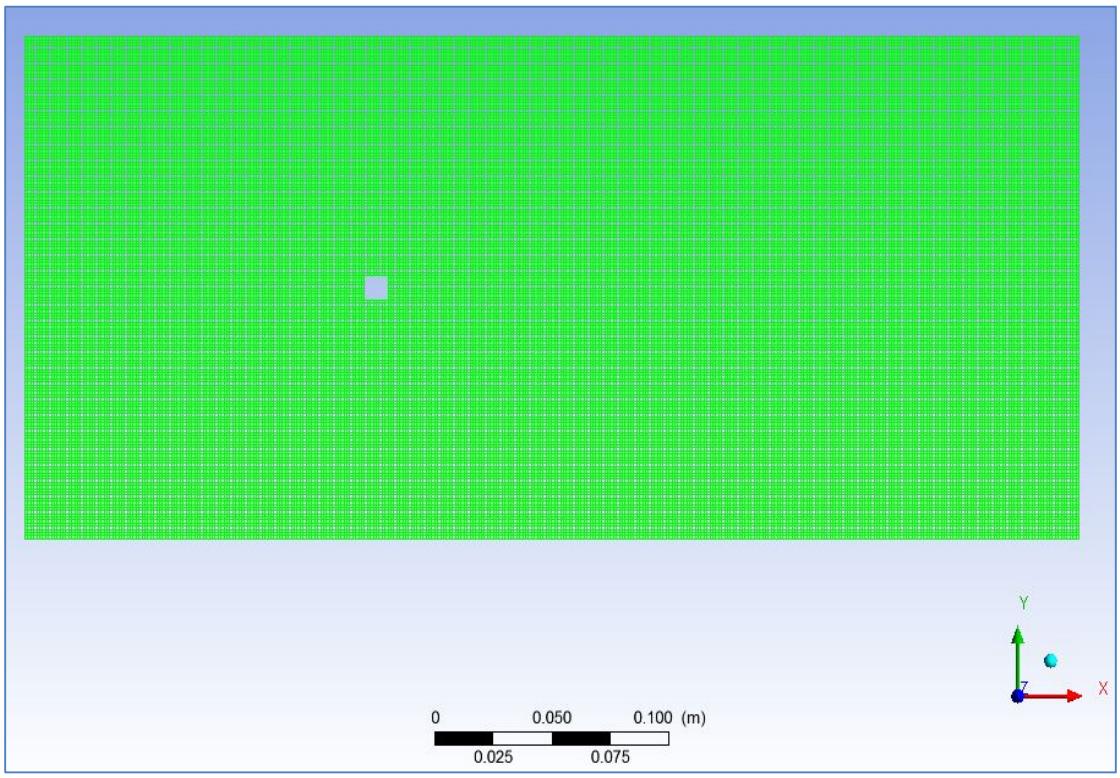

Figure 3.3. Mesh created in Gambit (Mesh X) for square cylinder problem.

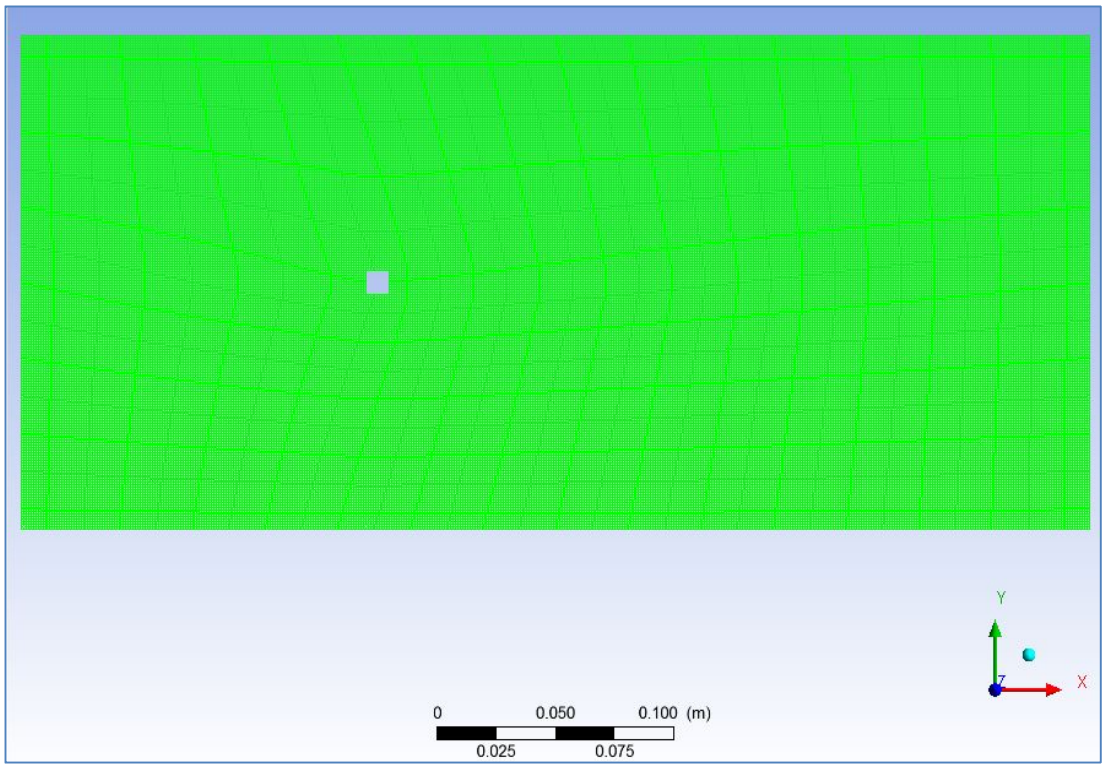

Figure 3.4. Mesh created in Gambit (Mesh Y) for square cylinder problem.

3.2. Problem Input Parameters

After defining the geometry of the domain and generating the mesh in this domain, the following steps are the definition of the problem in Polyflow program and inserting the input parameters for Newtonian, Generalized Newtonian (Power-law) and differential viscoelastic fluid (FENE-P) models.

In Newtonian fluid model, the viscosity is taken as constant $\mu = 0.001003$ Pa·s in order to simulate tap water flow. In Power-law fluid model, three different polymer concentrations are simulated in consideration of the rheological properties of a polymer type, which is called as 'Flopam AN 913 SH'. 20 wppm (weight parts per million), 40 wppm and 80 wppm concentrations are simulated using the input from rheometer measurements. The Power-law fluid model parameters are fixed according to the experimental data by means of curve fitting [45]. In FENE-P model simulations, the Weissenberg Number (where $We = \lambda V/d$) and

polymer chain extensibility *L* are varied in order to represent different polymer concentrations. Table 3.1 shows a summary of all simulations in terms of fluid properties. Circular cylinder problem solution includes Newtonian, Power-law and Viscoelastic fluid models simulations whereas square cylinder problem solution includes Newtonian and Power-law fluid models only.

Table 3.1. Input parameters for fluid models.

Newtonian	*Viscoelastic*		*Power-law*		
Viscosity (Pa·s)	*We*	*L*	*Viscosity (Pa·s)*	*n*	*m*
1.003×10^{-3}	0.01	10	0.91×10^{-3}	0.95	1.26
	0.03	10	0.92×10^{-3}	0.93	1.55
	0.05	10	0.99×10^{-3}	0.89	2.14
	0.01	30			
	0.03	30			
	0.05	30			

In addition to fluid model parameters, shown in Table 3.1, the Reynolds number *Re* is varied from 200 to 4000 in circular cylinder simulations.

Apart from the input parameters of flow models, related to fluid and flow properties; there are some other aspects which need to be taken into consideration while defining the simulation such as iterative time step range, maximum number of iterations and tolerance value for time-dependent simulations.

3.3. Mesh Independency

Mesh independency is a vital point in finite element studies, as well as mesh generation. It is required in order to ensure that correct solution of the problem is maintained regardless of the grid size. Mesh independency control has been performed with 1% error band for drag coefficient and vortex formation length in Newtonian simulations of both circular and square cylinder problems.

3.3.1. Mesh Independency of Circular Cylinder Problem

Mesh independency analysis has been performed in parallel with all Newtonian simulations of circular cylinder; by comparing Reynolds number and vortex formation length results for different meshes. In Newtonian simulations for circular cylinder problem, mesh A and mesh B converge properly and give more or less the same results (less than 1% difference), up to *Re* = 3500. For *Re* = 3500, the solution with the coarser mesh (i.e. Mesh A) could not converge. Hence, the simulations with *Re* = 3500 and *Re* = 4000 have been run with Mesh B and Mesh C. The drag coefficient and vortex formation length results of Newtonian simulations with Mesh B and Mesh C have given almost the same results (within 1% error band); as shown in Figure 3.5 and 3.6 where Error-1 means the percentage difference between Mesh A and Mesh B; whereas Error-2 indicates the difference between Mesh B and Mesh C.

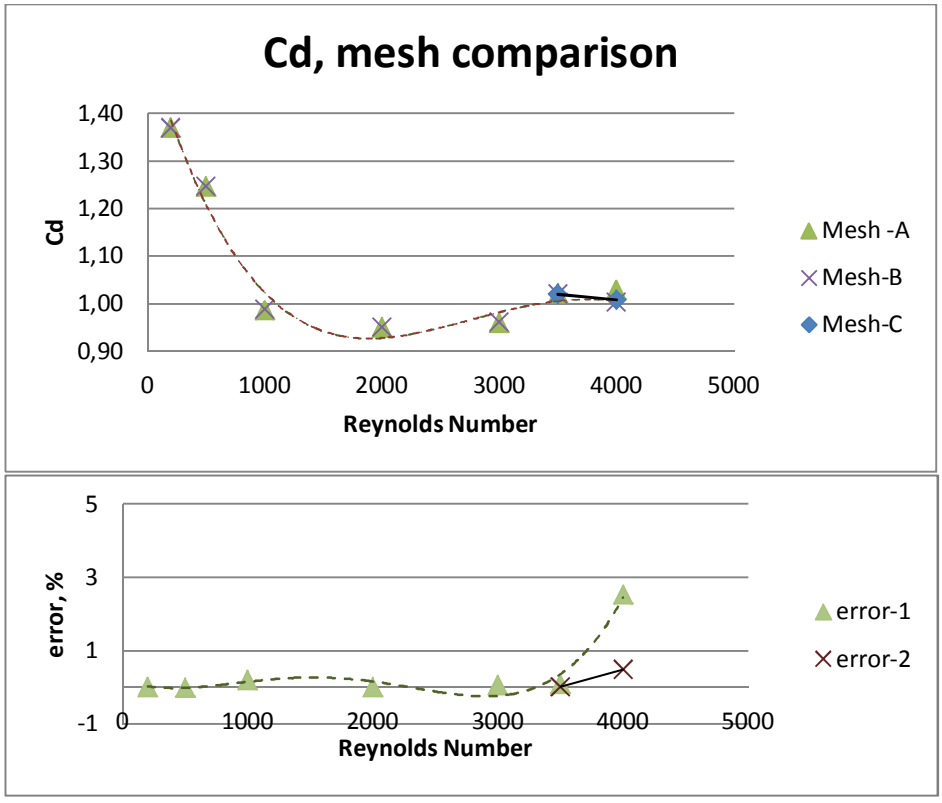

Figure 3.5. Mesh independency analysis for circular cylinder (drag coefficient versus Reynolds number).

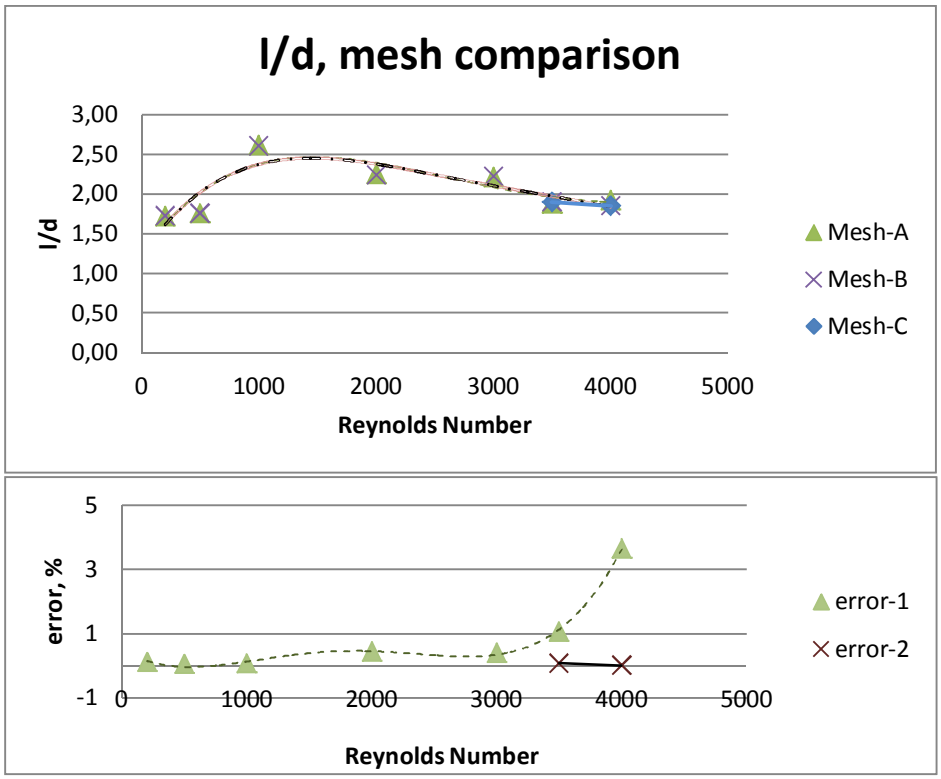

Figure 3.6. Mesh independency analysis for circular cylinder (vortex formation length versus Reynolds number).

3.3.2. Mesh Independency of Square Cylinder Problem

Similar to the circular cylinder mesh independency check, square circular simulations are also verified, in terms of mesh independency, by comparing Reynolds number and vortex formation length results of Newtonian simulations for different meshes. Figures 3.7 and 3.8 show drag coefficient and vortex formation length comparison between Mesh X and Mesh Y, described previously. Both parameters show difference of less than 1 percent.

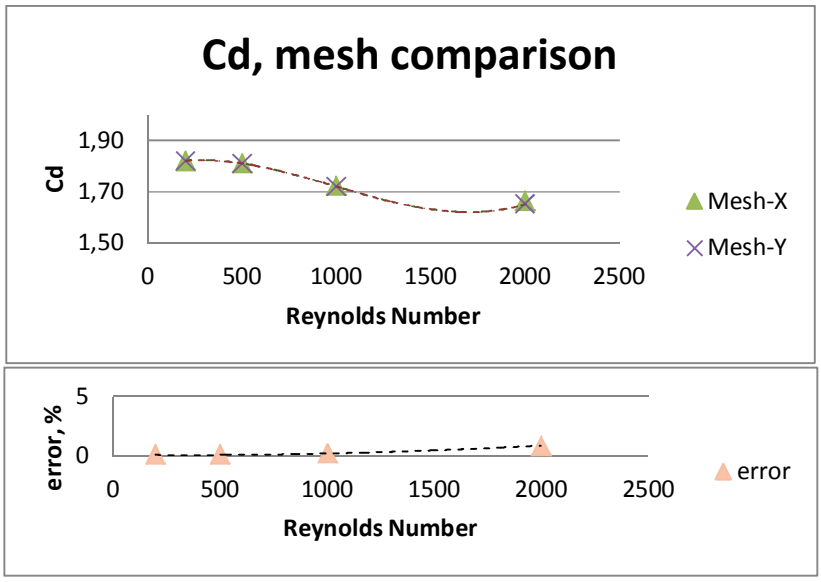

Figure 3.7. Mesh Independency Analysis for Square Cylinder (drag coefficient versus Reynolds number).

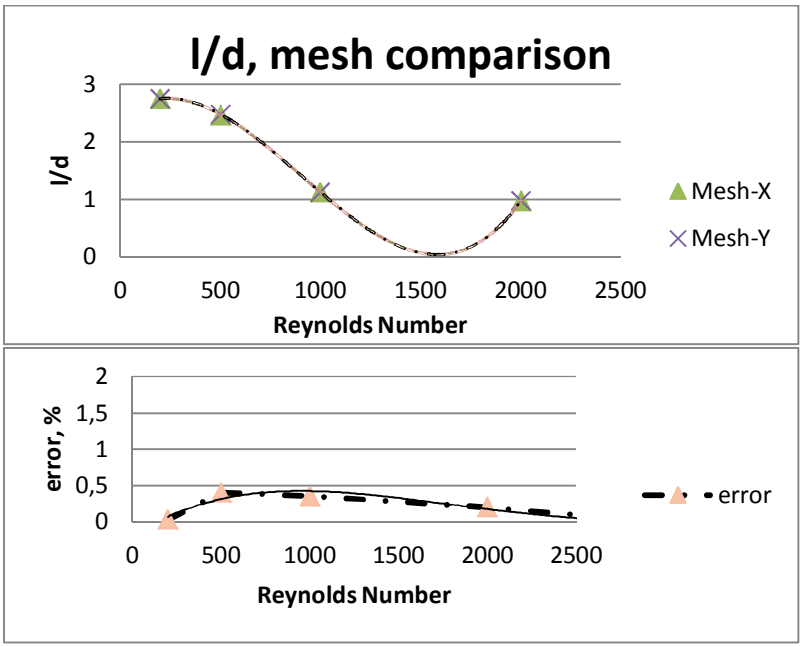

Figure 3.8. Mesh Independency Analysis for Square Cylinder (vortex formation length versus Reynolds number).

3.4. Convergence

Since the simulations are time dependent, periodic solution patterns are observed. These time-dependent periodic solutions are then time-averaged in post-processing, by means of CFD-Post post processing tool, to calculate the flow parameters of the problem. In Figure 3.10 and Figure 3.11, for Mesh A and Mesh B respectively, convergence of the velocity component for a Newtonian simulation results are shown at two arbitrary points (Point 1 and Point 2, as shown in Figure 3.9) in the wake region of the cylinder, where Reynolds number equals to 1000.

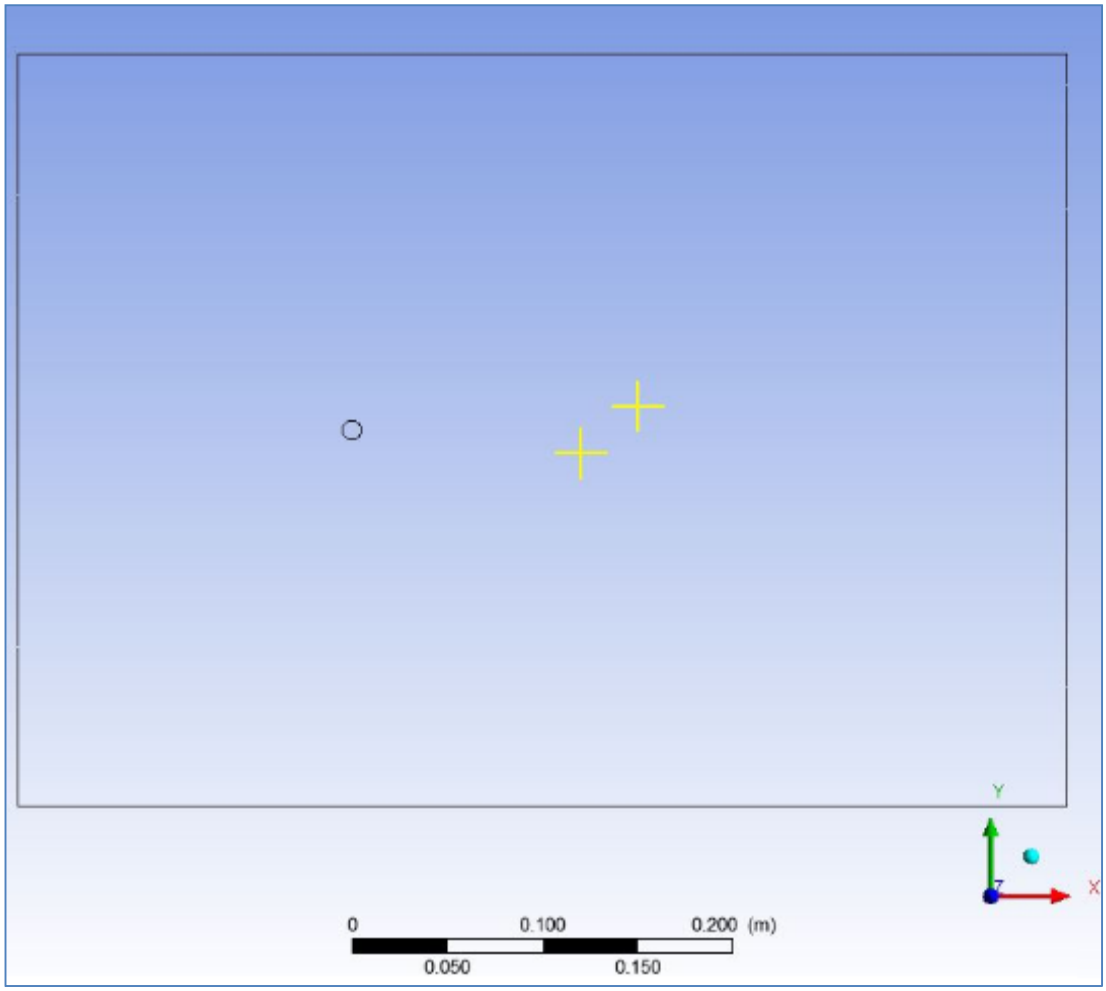

Figure 3.9. Position of two arbitrary points (Point 1 and Point 2) in the domain.

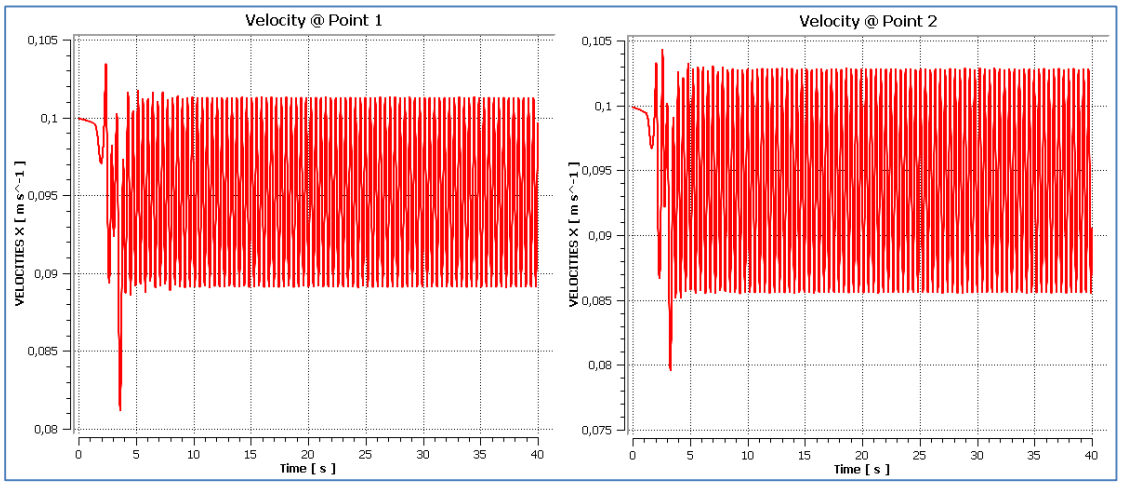

Figure 3.10. Longitudinal velocity component versus time graph at two arbitrary points (Point 1 and Point 2) in wake region, *Re* = 1000 (Mesh A).

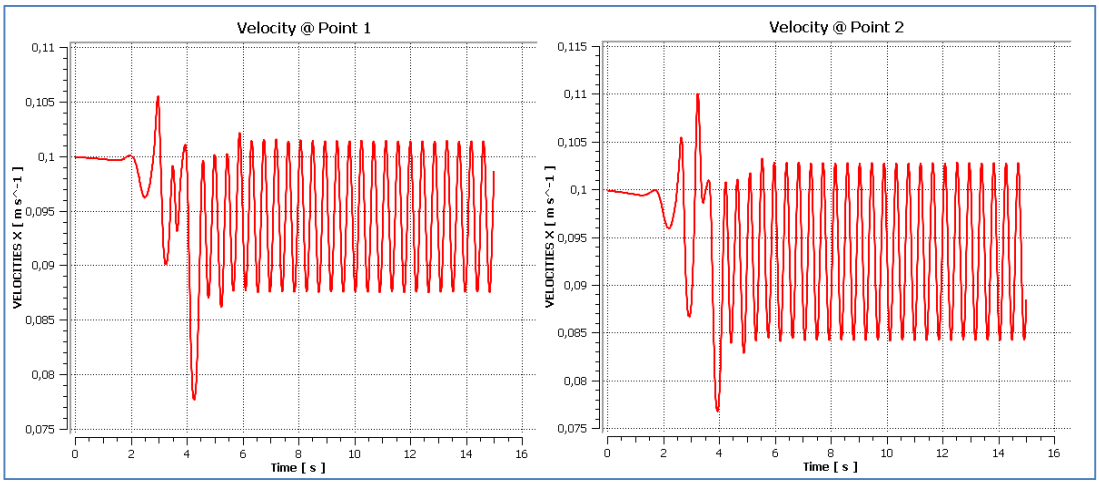

Figure 3.11. Longitudinal velocity component versus time graph at two arbitrary points (Point 1 and Point 2) in wake region, Re = 1000 (Mesh B).

It is obviously seen that each velocity graph converges to a periodic solution after the same time step for each point; around t = 8 sec. for Mesh A and around t = 6 sec. for Mesh B. The time-averaging in post-processing of the simulation is done within t = 8-10 sec. for Mesh A and within t = 6-8 for Mesh B. Moreover, it is seen that for the finer mesh (Mesh B), the simulation converges at an early time.

Figure 3.12and Figure 3.13 also show similar solutions for *Re* = 500, (meshes and points are the same). Velocity component value converges around *t* = 18 seconds for Mesh A and *t* = 15 seconds for Mesh B.

A similar convergence study has been carried out for each circular and square cylinder simulation case during post-processing.

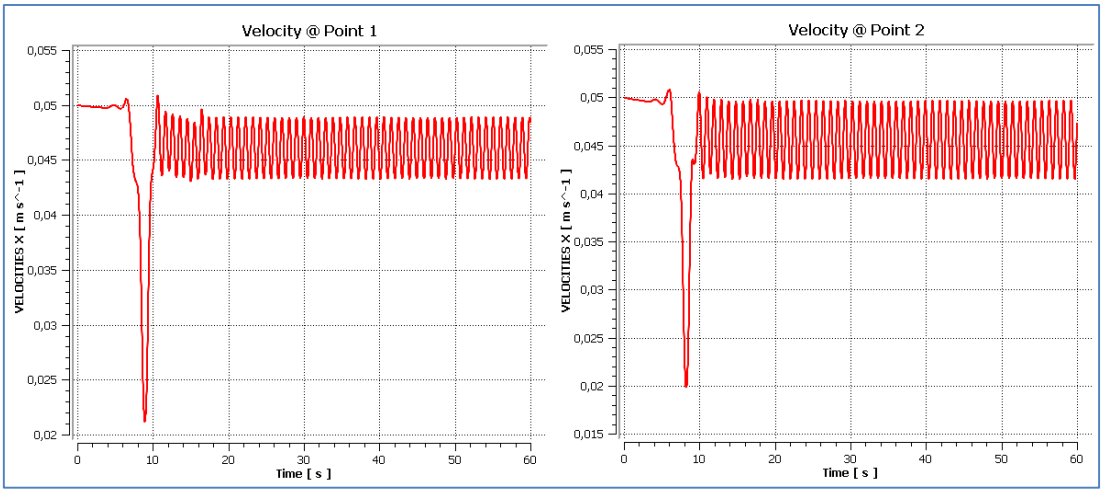

Figure 3.12. Longitudinal velocity component versus time graph at two arbitrary points (Point 1 and Point 2) in wake region, *Re* = 500 (Mesh A).

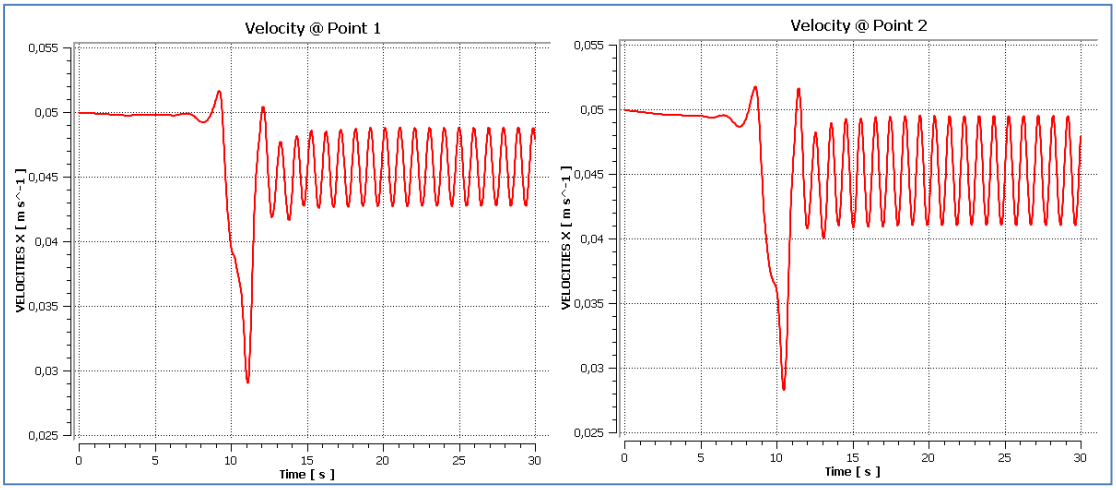

Figure 3.13. Longitudinal velocity component versus time graph at two arbitrary points (Point 1 and Point 2) in wake region, Re = 500 (Mesh B).

Computational time, also called as running time, is the length of time required to perform a computational process. Considering a computation as a sequence of rule applications, the computation time is proportional to the number of rule applications. In the simplest of terms, it is possible to divide the task of a processor into a number of processors, which is called as parallel processing and the most obvious benefit of using a parallel processing is the reduction in the running time of the code. Therefore, a straightforward measure of the parallel performance would be the ratio of the computational time on a single processor to that on a multiprocessor [46].

In this study, for the solution of polymer induced flow around circular and square cylinders, Polyflow program is used, by means of five processors working in parallel. The computer time of the simulations is varied from 30 minutes up to 103 hours. The parallel performance of the processors has prevented the need for longer computer time during simulations.

4. RESULTS AND DISCUSSIONS

This section of the thesis consists of the presentation of numerical solutions in terms of flow properties, such as drag coefficient, vortex formation length, vortex shedding frequency, and wake region velocity distribution for both circular and square cylinder simulations. The simulations, are also compared with literature and recent studies to understand the effects of polymer addition on flow around circular and square cylinders.

4.1. Drag Coefficient

In experimental and numerical studies, the calculation of the drag coefficient by considering mean velocity values and velocity fluctuations is much simpler than integrating the traction force component over the body. Hence, Rajagopalan's formula [47], given below, will be applied on the line located around 30 diameters distance away from the center of cylinder in the wake region in order to calculate the drag coefficient:

$$C_d = 2\int_{-\infty}^{\infty} \frac{U}{V}\left(\frac{V-U}{V}\right) d\left(\frac{y}{d}\right) + 2\int_{-\infty}^{\infty} \left(\frac{\overline{v^2}-\overline{u^2}}{V^2}\right) d\left(\frac{y}{d}\right) \qquad (4.1)$$

where V is the freestream velocity, U is the local mean longitudinal velocity component, u and v are longitudinal and lateral velocity fluctuations, and d is the characteristic length of the cylinder, i.e. diameter of the circular cylinder or side of the square cylinder.

As Rajagopalan's integral formula is applied at a location far enough from the cylinder; the second integral, which represents the effect of fluctuations, is neglected compared to the first integral. And; the first integral is calculated by taking root mean square of velocity values of each point.

4.1.1. Drag Coefficient in Circular Cylinder Problem

During post-processing of the data for circular cylinder problem, the integral formula is applied at 30 diameter distance away from the cylinder; and 57 vertical points are located, as shown in Figure 4.1, to simulate the integral by means of trapezoidal rule.

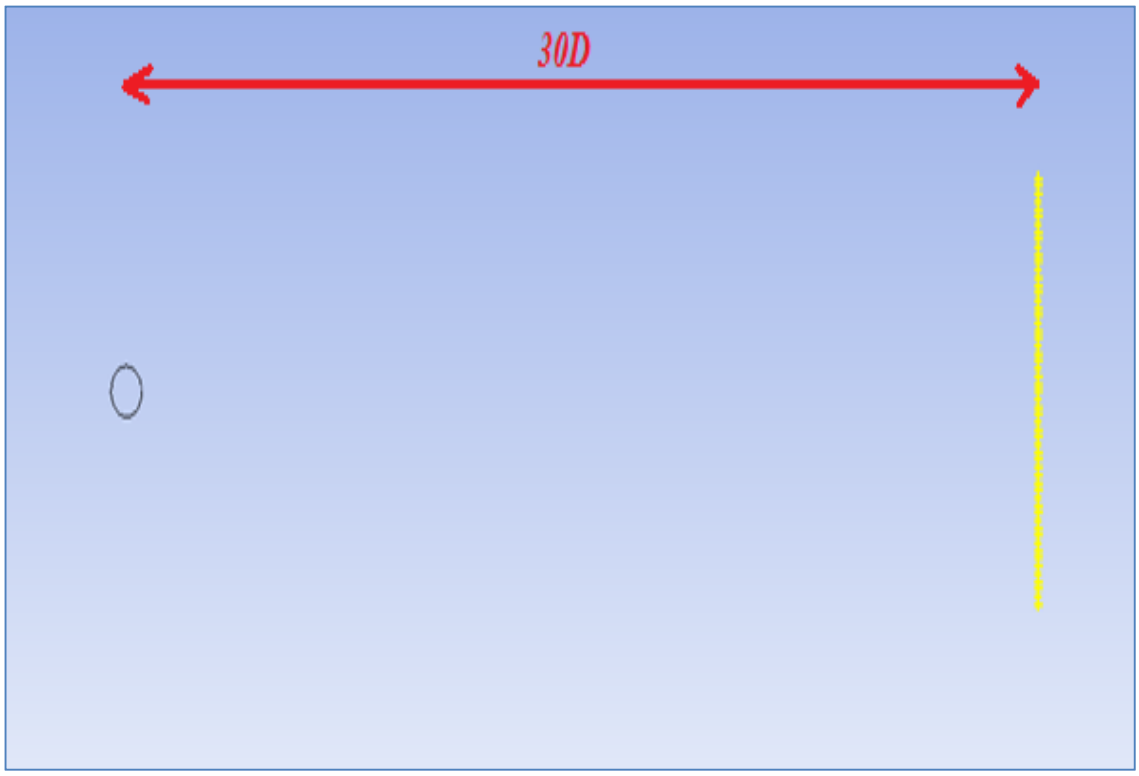

Figure 4.1. Vertical points located in circular cylinder problem domain for Rajagopalan's drag coefficient integral.

In terms of consistency with the literature, comparison with drag coefficient values in literature obtained for flow around circular cylinders of Newtonian fluid would be useful for validation of the results.. For instance, the drag coefficient values obtained by Wieselsberger [48], as shown in Figure 4.2, is a good reference for comparison.

Figure 4.3 shows the drag coefficient trend with respect to Reynolds number for Newtonian fluid flow around circular cylinder, in this study. Figure 4.4 shows the comparison between Newtonian simulations results of circular cylinder problem and Wieselsberger's results, in terms of drag coefficient. The results are in good agreement with these reference

values, except *Re* = 200. The drag coefficient is deduced as 1.37 at *Re* = 200 in this study whereas it is 1.7, according to Wieselsberger's results.

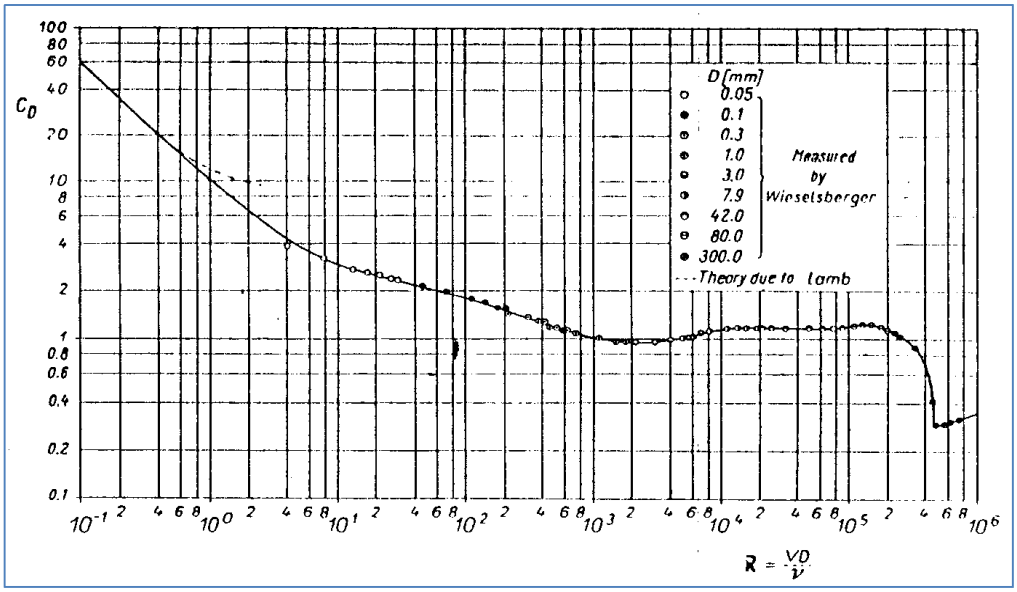

Figure 4.2. Wieselsberger's drag coefficient trend for flow around circular cylinders [48].

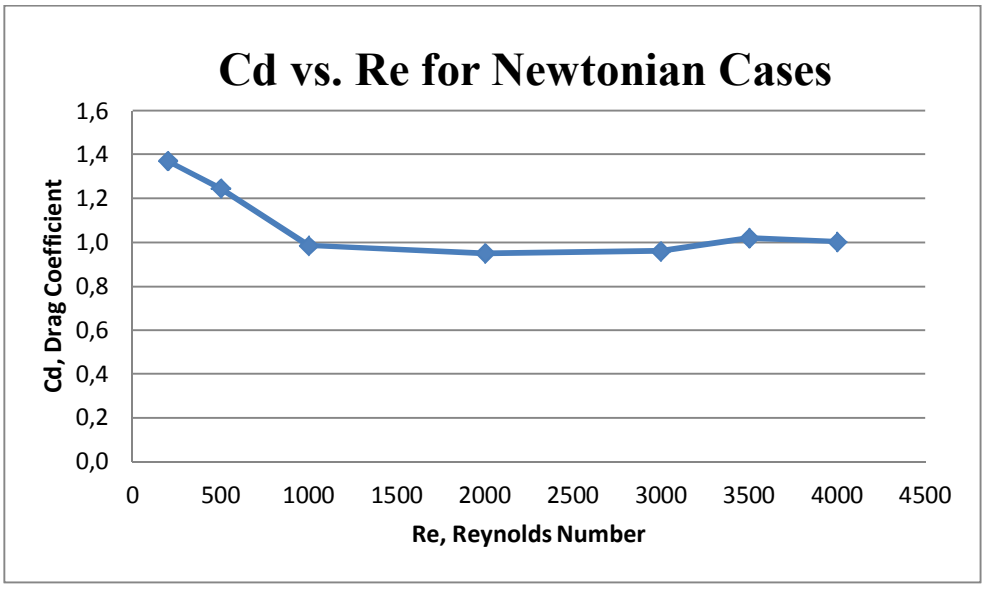

Figure 4.3. Circular cylinder problem drag coefficient vs. Reynolds number graph for Newtonian flow.

As shown in Figure 4.4, there is a similar convergence seen in Newtonian simulations results and Wieselsberger's results, except *Re* =3500; i.e. the drag coefficient gets higher than 1 and decreases to a value lower than 1 again. Hence, to be consistent with Wieselsberger's results, the drag coefficient is taken as 1.7 and 0.96, at *Re* = 200 and *Re* = 3500 respectively, in the rest of the study.

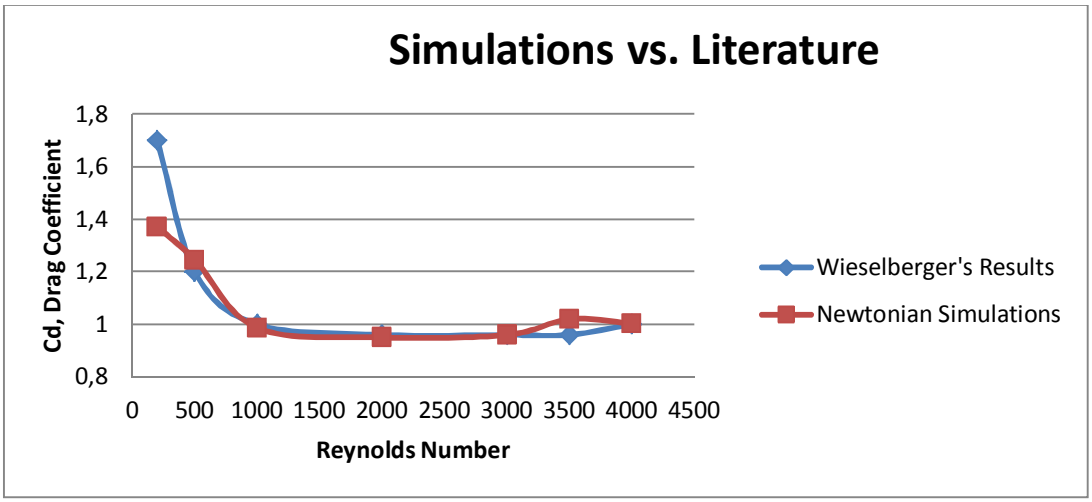

Figure 4.4. Circular cylinder drag coefficient comparison with Weisselberger's results.

Table 4.1 shows the effect of polymer addition on drag reduction, using differential viscoelastic model FENE-P. The Weissenberg number is varied from 0.01 to 0.03, the polymer chain length is varied from 10 to 30 and the Reynolds number is varied from 200 to 4000.

Table 4.1. Drag coefficient in circular cylinder viscoelastic simulations (FENE-P model).

C_d	*Newtonian*	*We = 0.01 L = 10*	*We = 0.03 L = 10*	*We = 0.05 L = 10*	*We = 0.01 L = 30*	*We =0.03 L=30*	*We=0.05 L=30*
Re = 200	1.700	1.370	1.358	1.377	1.376	1.421	1.372
Re = 500	1.246	1.259	1.268	1.276	1.261	1.272	1.281
Re = 1000	0.986	0.996	1.012	1.024	1.028	1.029	1.033
Re = 2000	0.950	0.990	0.993	0.998	0.972	0.987	0.996
Re = 3000	0.960	1.002	1.030	1.022	1.028	1.010	1.004
Re = 3500	0.960	1.006	1.006	1.001	1.010	1.011	1.003
Re = 4000	1.003	1.009	1.015	1.011	1.011	1.003	1.004

According to the drag coefficient results shown in Table 4.1, the drag coefficient has a sharp reduction with increasing polymer addition at Re = 200, compared to Newtonian fluid. For 200 < $Re \leq$ 3000, there is an increasing trend in drag reduction with increasing We and L. On the other hand, there is no significant changing trend for 3500 $\leq Re \leq$ 4000.

Table 4.2. Drag coefficient in circular cylinder Power-law simulations.

C_d	Newtonian	20 wppm	40 wppm	80 wppm
Re = 200	1.700	1.367	1.363	1.350
Re = 500	1.246	1.167	1.136	1.084
Re = 1000	0.986	0.881	0.860	0.840
Re = 2000	0.950	0.979	0.972	1.098
Re = 3000	0.960	0.953	0.951	0.942
Re = 3500	0.960	1.005	1.001	0.981
Re = 4000	1.003	0.992	0.989	0.972

Table 4.2 shows the effect of polymer addition on drag, using Generalized Newtonian fluid (Power-law) model, for the same Reynolds number range. Drag coefficient has a decaying trend for Power-law simulations with increasing polymer concentration, except Re = 2000 *and* Re = 3500, compared to Newtonian cases. This can lead to the conclusion that polymer addition creates a drag reduction, with respect to Power-law fluid model, around circular cylinder.

4.1.2. Drag Coefficient in Square Cylinder Problem

Similar to the circular cylinder drag coefficient calculations, Rajagopalan's C_d Integral formula is applied at 25 diameter distance away from the square cylinder; and 57 vertical points are located, as seen in Figure 4.5.

Figure 4.7 shows that the drag coefficient results of square cylinder Newtonian simulations are in parallel with results of previous studies [49].

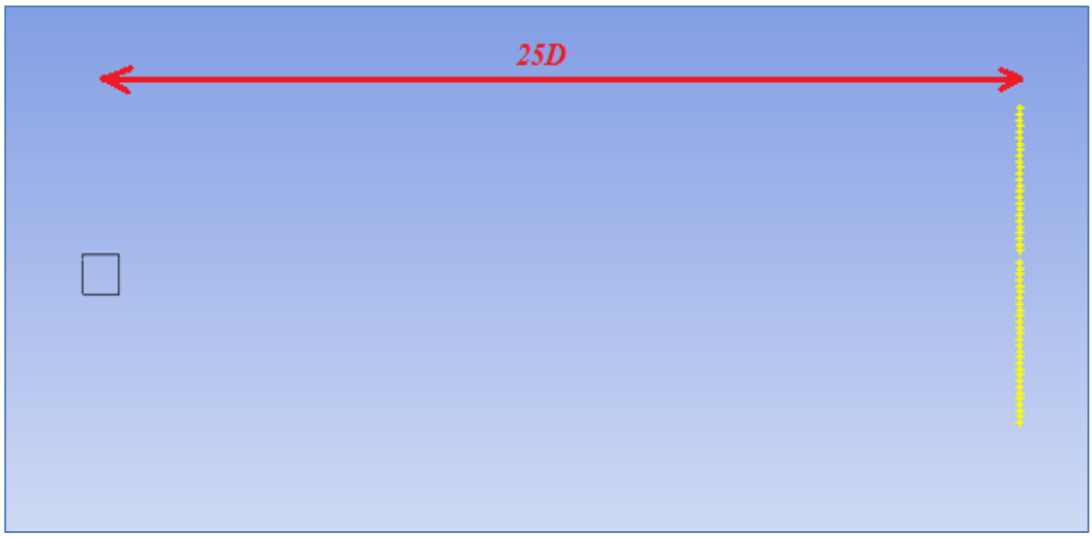

Figure 4.5. Vertical points located in square cylinder problem domain for Rajagopalan's drag coefficient integral.

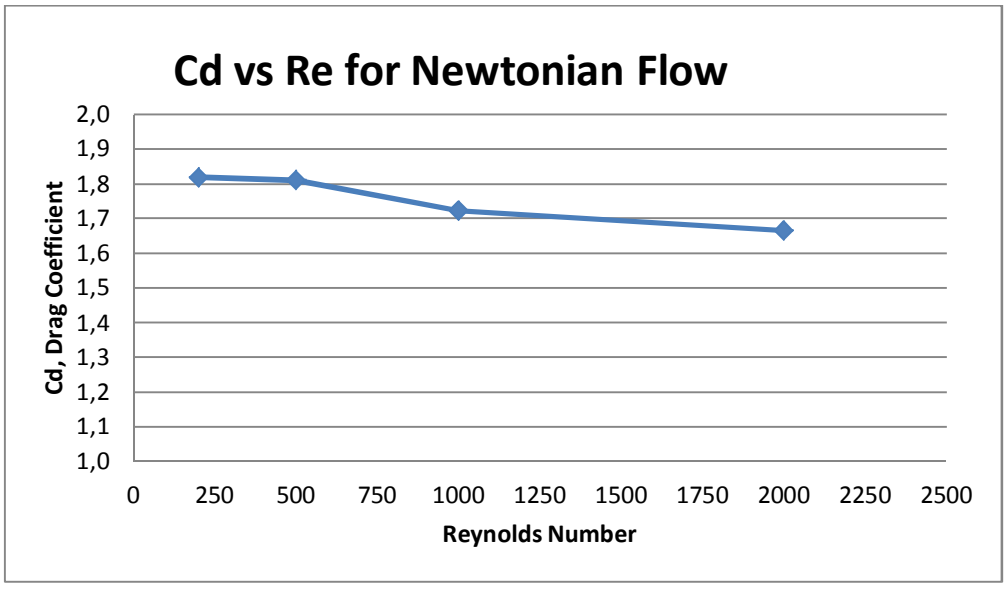

Figure 4.6. Square cylinder problem drag coefficient vs. Reynolds number graph for Newtonian flow.

Table 4.3 represents the effect of polymer addition on drag coefficient for flow around square cylinder, compared to Newtonian case, using Power-law fluid model in the Reynolds number range from $Re = 200$ to $Re = 2000$.

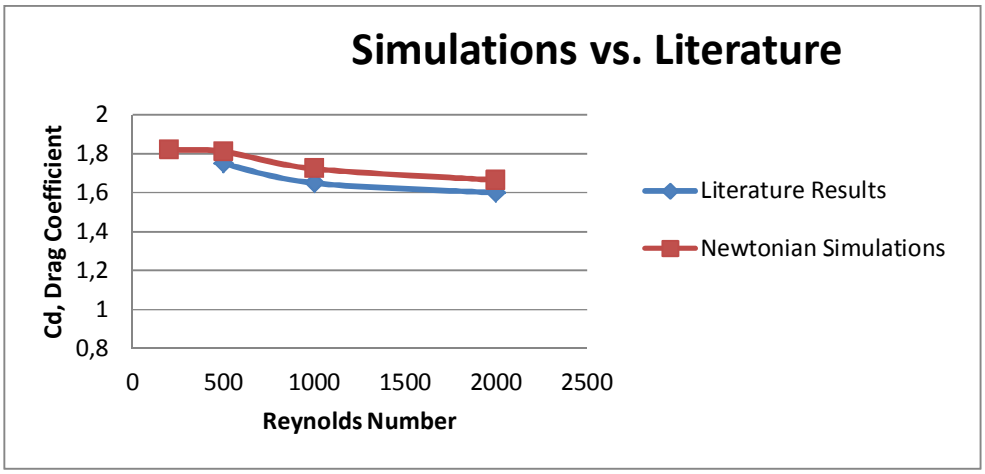

Figure 4.7. Square cylinder drag coefficient comparison with literature results.

Table 4.3. Drag coefficient in square cylinder Power-law simulations.

C_d	*Newtonian*	*20 wppm*	*40 wppm*	*80 wppm*
$Re = 200$	1.819	1.802	1.801	1.794
$Re = 500$	1.811	1.799	1.770	1.763
$Re = 1000$	1.723	1.708	1.674	1.610
$Re = 2000$	1.665	1.606	1.522	1.412

It is observed that the drag coefficient reduces with polymer addition. The amount of the drag reduction increases at high Reynolds numbers; for example drag reduction increases up to 0.25 with polymer addition when $Re = 2000$.

4.2. Vortex Formation Length

4.2.1. Vortex Formation Length in Circular Cylinder Problem

We first compare the vortex formation length results with the available data in the literature for the Newtonian case. In Figures 4.9 - 4.14, the vorticity profiles are visualized for Reynolds number range from $Re = 200$ to $Re = 4000$.

Figure 4.8. Circular cylinder wake region vorticity profile, Newtonian fluid (*Re* = 200).

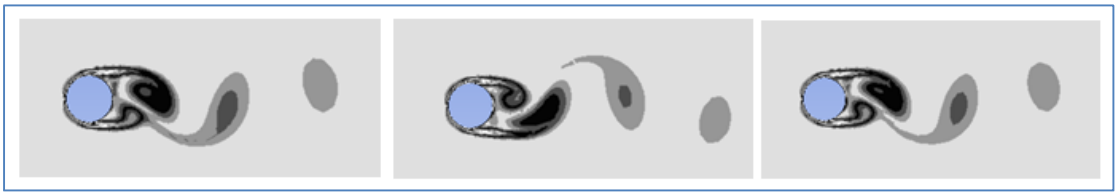

Figure 4.9. Circular cylinder wake region vorticity profile, Newtonian fluid (*Re* = 500).

Figure 4.10. Circular cylinder wake region vorticity profile, Newtonian fluid (*Re* = 1000).

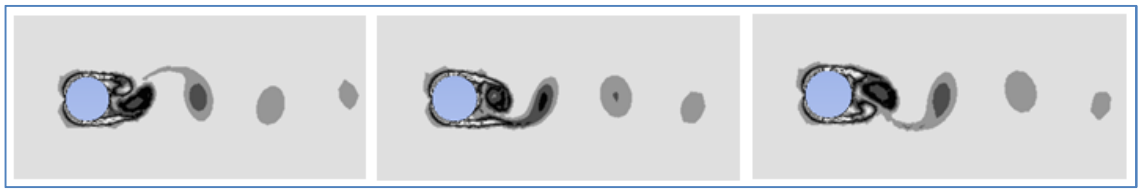

Figure 4.11. Circular cylinder wake region vorticity profile, Newtonian fluid (*Re* = 2000).

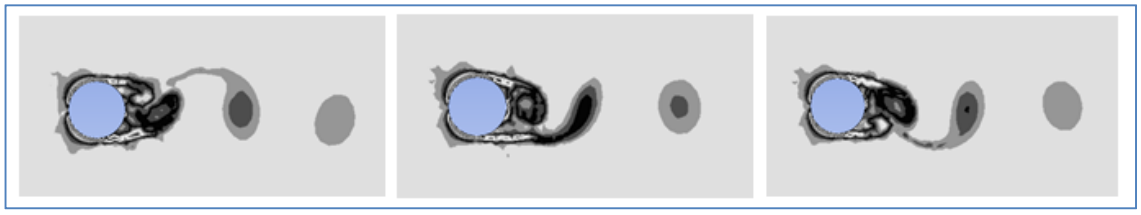

Figure 4.12. Circular cylinder wake region vorticity profile, Newtonian fluid (*Re* = 3000).

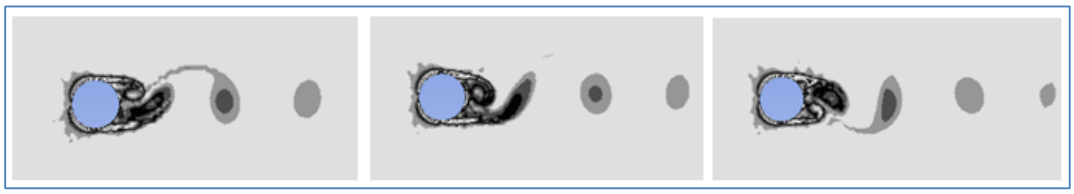

Figure 4.13. Circular cylinder wake region vorticity profile, Newtonian fluid (Re = 3500).

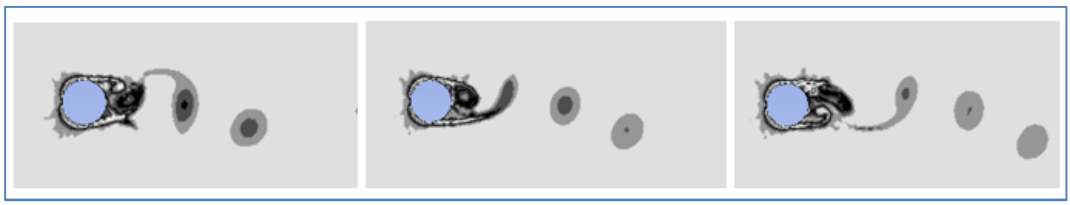

Figure 4.14. Circular cylinder wake region vorticity profile, Newtonian fluid (Re = 4000).

Figures 4.15 visualizes the vorticity profile of Power-law fluid, which simulates 40 wppm polymer concentration at Re = 200; and Figure 4.16 visualizes the vorticity profile of FENE-P model, in which We = 0.05 and L = 10 at Re = 200.

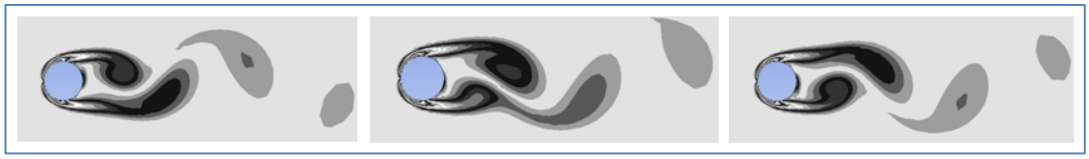

Figure 4.15. Circular cylinder wake region vorticity profile, Power-law fluid (80 wppm, Re = 200).

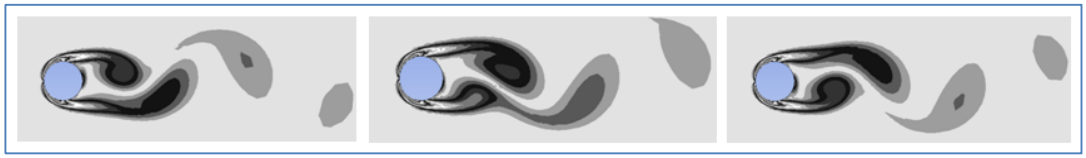

Figure 4.16. Circular cylinder wake region vorticity profile, viscoelastic FENE-P model (We = 0.05, L = 30, Re = 200).

Figures 4.17 visualizes the vorticity profile of Power-law fluid, which simulates 80 wppm polymer concentration at Re = 500; and Figure 4.18 visualizes the vorticity profile of FENE-P model, in which We = 0.05 and L = 30 at Re = 500.

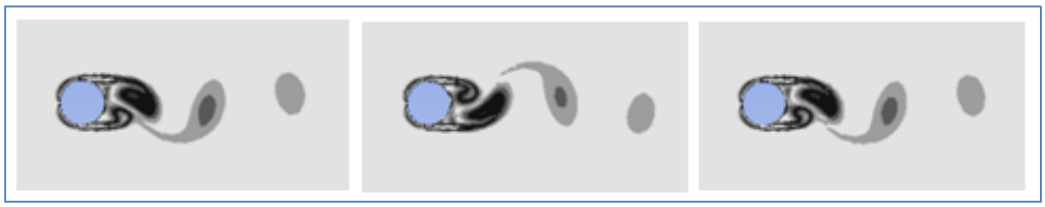

Figure 4.17. Circular cylinder wake region vorticity profile, Power-law fluid (80 wppm, $Re = 500$).

Figure 4.18. Circular cylinder wake region vorticity profile, viscoelastic FENE-P model ($We = 0.05$, $L = 30$, $Re = 500$).

Figure 4.19 shows the trend of the non-dimensional parameter *l/d* (ratio of vortex formation length to cylinder diameter) for all Newtonian fluid flow cases. The vortex formation length results of the studies of Gerrard, Peltzer and Woo [32] are given in Figure 4.19. With respect to Figures 4.19 and 4.20, it can be observed that the vortex formation length results for Newtonian cases are in agreement with the literature, in Reynolds number range from $Re = 200$ to $Re = 4000$.

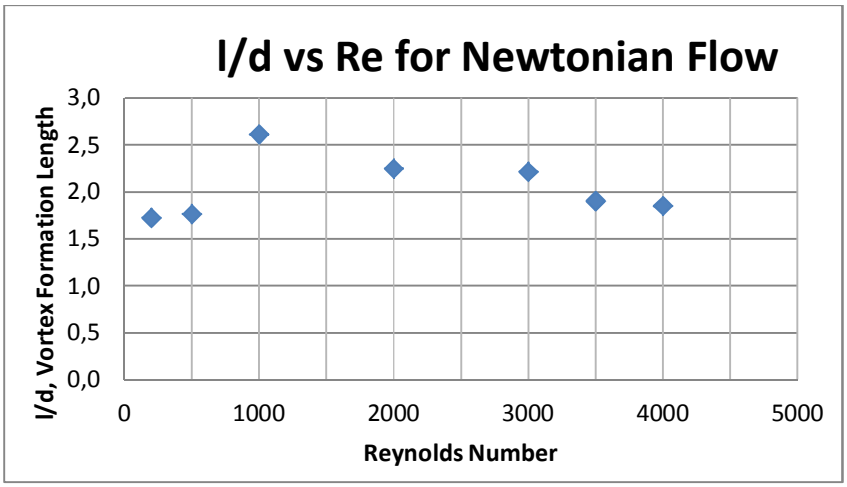

Figure 4.19. Vortex formation length vs. Reynolds number for Newtonian circular cylinder problem.

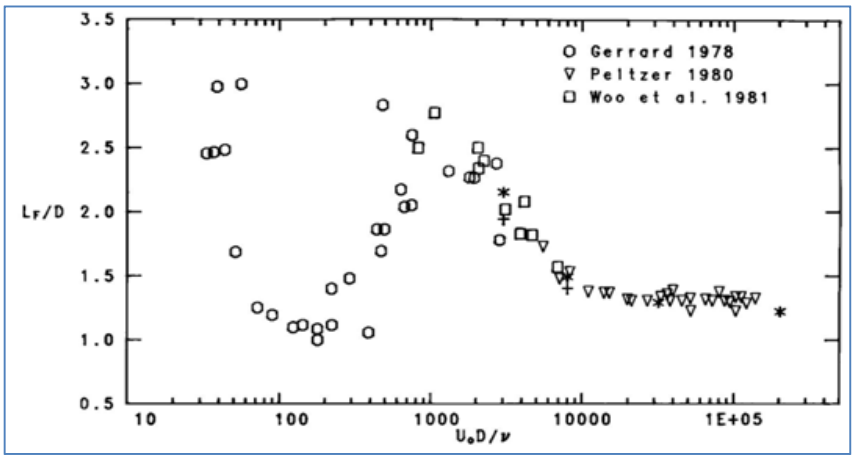

Figure 4.20. Vortex formation length vs. Reynolds number [32].

Table 4.4 and Table 4.5 show *l/d* trends for viscoelastic FENE-P and Generalized Newtonian fluid model simulations for varying Reynolds numbers, compared to Newtonian results.

Table 4.4. Circular cylinder vortex formation length in viscoelastic simulations (FENE-P).

l/d	*Newtonian*	*We = 0.01 L = 10*	*We = 0.03 L = 10*	*We = 0.05 L = 10*	*We = 0.01 L = 30*	*We =0.03 L=30*	*We=0.05 L=30*
Re = 200	1.72	1.719	1.715	1.715	1.72	1.6	1.72
Re = 500	1.76	1.54	1.56	1.65	1.65	1.65	1.55
Re = 1000	2.61	2.50	2.52	2.51	2.50	2.49	2.5
Re = 2000	2.25	2.21	2.208	2.22	2.21	2.217	2.21
Re = 3000	2.22	2.19	2.149	2.16	2.158	2.2	2.19
Re = 3500	1.90	1.92	1.92	1.929	1.93	1.93	1.942
Re = 4000	1.85	1.843	1.841	1.843	1.842	1.845	1.845

Table 4.5. Circular cylinder vortex formation length in Power-law simulations.

l/d	*Newtonian*	*20 wppm*	*40 wppm*	*80 wppm*
Re = 200	1.72	1.22	1.17	1.08
Re = 500	1.76	1.56	1.35	1.35
Re = 1000	2.61	2.5	2.36	2.31
Re = 2000	2.25	2.198	2.213	2.181
Re = 3000	2.22	2.229	2.235	2.237
Re = 3500	1.90	1.908	1.912	1.92
Re = 4000	1.85	1.851	1.86	1.863

Table 4.4 shows that the vortex formation length decreases with increasing viscoelastic property, compared to Newtonian simulations, except Re = 3500. For Re = 3500, l/d increases with increasing viscoelastic property. Table 4.5 shows that the vortex formation length has a decreasing trend for Re < 3000 with polymer addition; whereas there is an increasing trend with polymer addition for $Re \geq 3000$.

4.2.2. Vortex Formation Length in Square Cylinder Problem

Figures 4.21 - 4.24 show instantaneous vorticity profiles for square cylinder Newtonian simulations. It is obvious that the geometric shape of the square, with corners, creates significant flow differences, compared to the circular cylinder, as Reynolds numbers increase. The vortices in the frontal area of the square get larger, as the effect of inertia increases compared to viscous effects. Another difference is the increasing instabilities in the wake region at higher Reynolds numbers.

Figure 4.21. Square cylinder wake region vorticity profile, Newtonian Fluid (Re = 200).

Figure 4.22. Square cylinder Wake region vorticity profile, Newtonian Fluid (Re = 500).

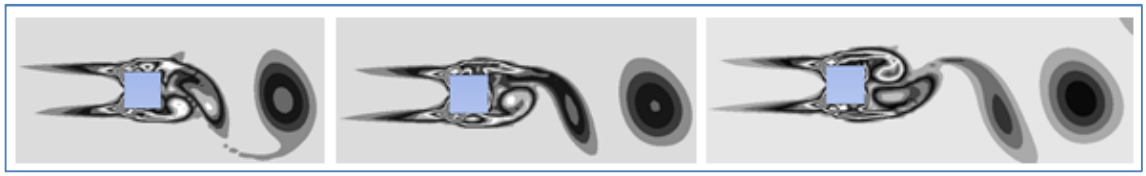

Figure 4.23. Square cylinder wake region vorticity profile, Newtonian Fluid (Re = 1000).

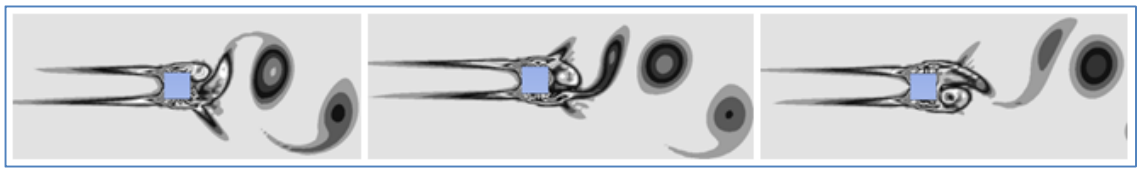

Figure 4.24. Square cylinder wake region vorticity profile, Newtonian Fluid (*Re* = 2000).

Figures 4.25 shows the wake region vorticity profile of a Power-law fluid model, which simulates 40 wppm polymer concentration at *Re* = 1000.

Figure 4.25. Square cylinder wake region vorticity profile, Power-law fluid model, 40 wppm (*Re* = 1000).

Table 4.6 represents the *l/d* results for all square cylinder simulations performed in this study. It is obviously seen that vortex formation length has a decreasing trend compared to Newtonian case for Power-law fluid model at *Re* = 200, *Re* = 500 and *Re* = 1000 whereas it increases for *Re* = 2000. It can be deduced that polymer addition creates a decrease in vortex formation length for high Reynolds number, and an increase in vortex formation length for low Reynolds numbers.

Table 4.6. Vortex formation length in square cylinder Power-law simulations.

l/d	*Newtonian*	*20 wppm*	*40 wppm*	*80 wppm*
Re = 200	2.75	2.71	2.60	2.60
Re = 500	2.47	2.44	2.41	2.37
Re = 1000	1.12	0.87	0.85	0.81
Re = 2000	0.97	1.14	1.22	1.25

4.3. Wake Region Velocity Distribution

Distribution of root mean square (RMS) velocities is another flow parameter which can be calculated by using the formula;

$$v_{rms} = \sqrt{\frac{{v_1}^2+{v_2}^2+{v_3}^2+\cdots+{v_n}^2}{n}} \tag{4.3}$$

where v_{rms} is the root mean square velocity, n is the number of time steps, and v_i is the longitudinal velocity component of a point at a time step, i.

4.3.1. Wake Region Velocity Distribution in Circular Cylinder Problem

Root mean square velocity distribution in the wake region of the circular cylinder for varying Reynolds numbers shown in Figures 4.27- 4.33. Figure 4.26 shows an instantaneous velocity vector distribution for Power-law fluid model that simulates 40 wppm polymer concentration at Re = 1000.

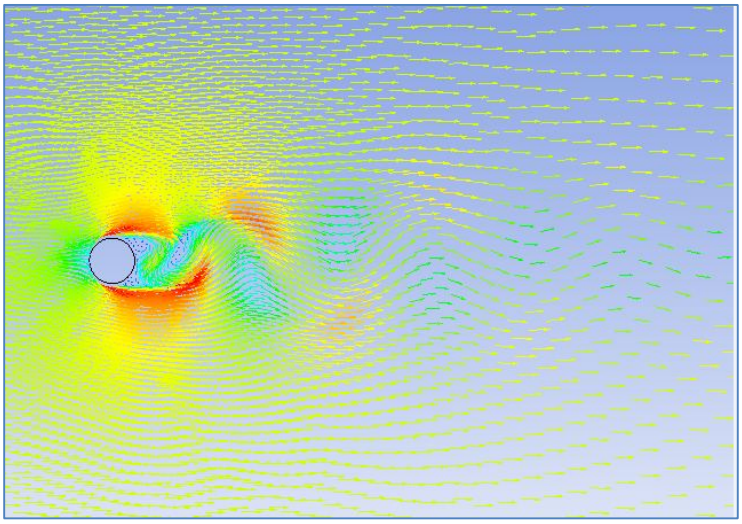

Figure 4.26. Instantaneous velocity vector distribution in circular cylinder problem domain, (Power-law fluid model, 40 wppm at Re = 1000).

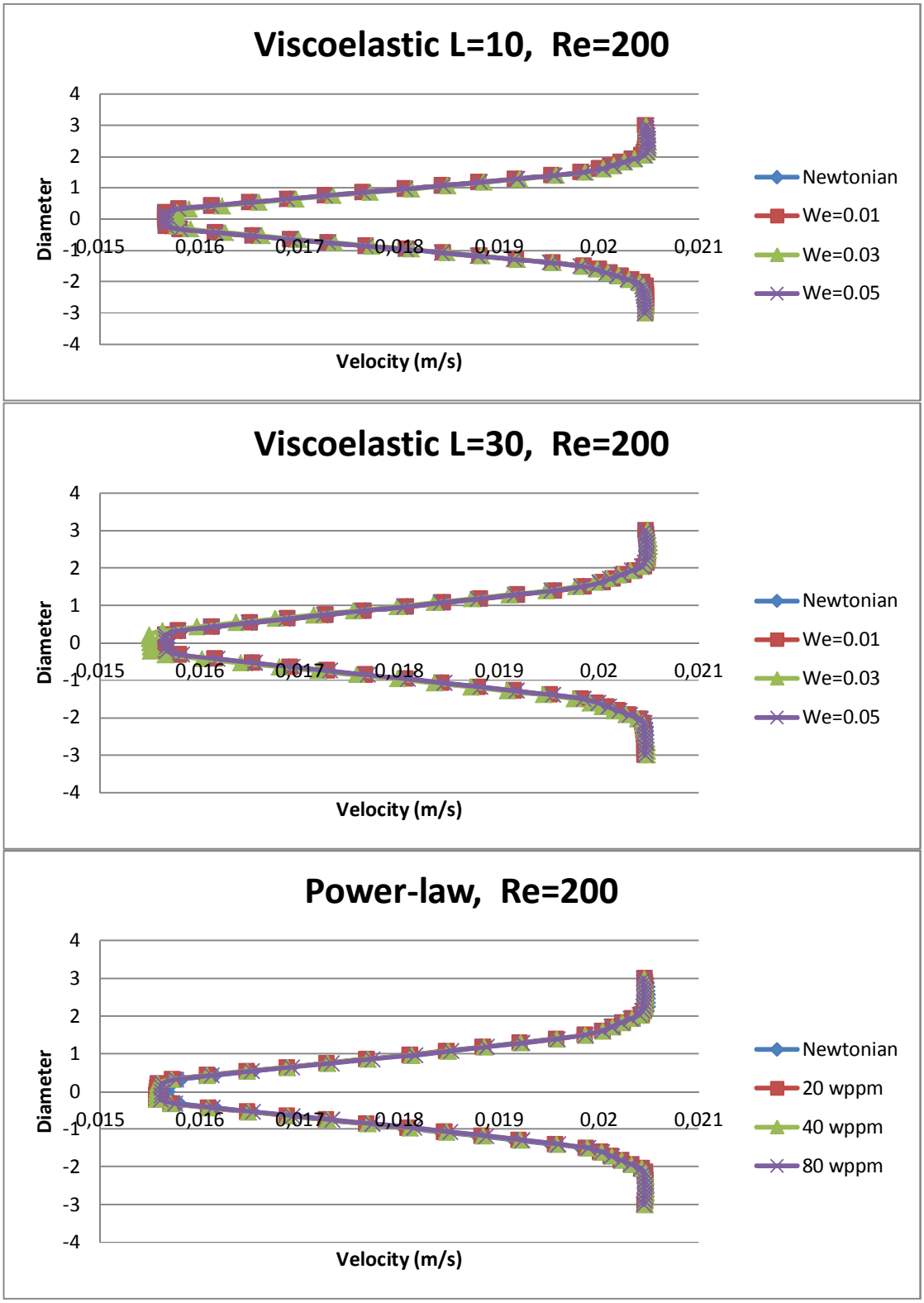

Figure 4.27. Circular cylinder wake region RMS velocity comparison for *Re* = 200.

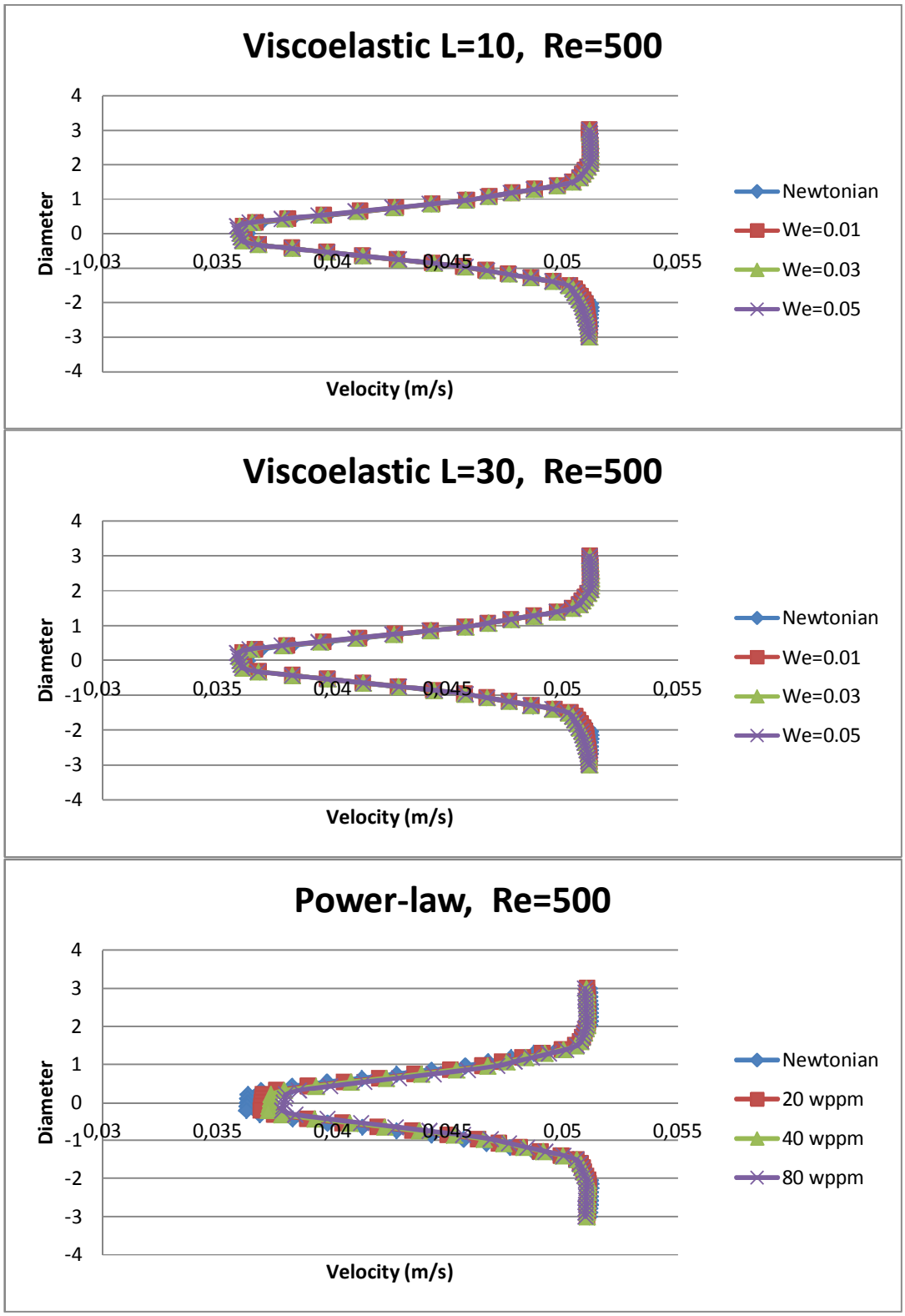

Figure 4.28. Circular cylinder wake region RMS velocity comparison for *Re* = 500.

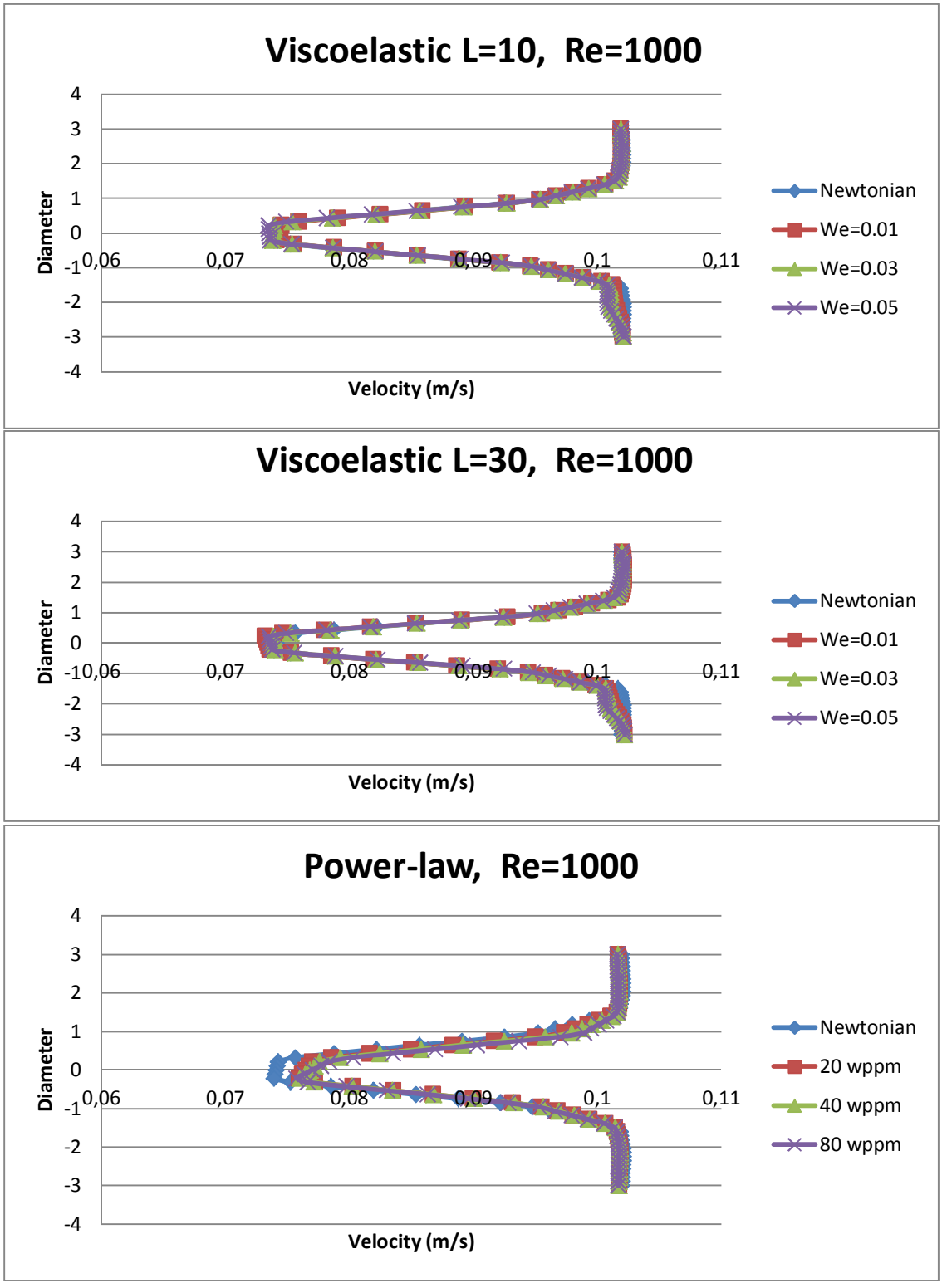

Figure 4.29. Circular cylinder wake region RMS velocity comparison for *Re* = 1000.

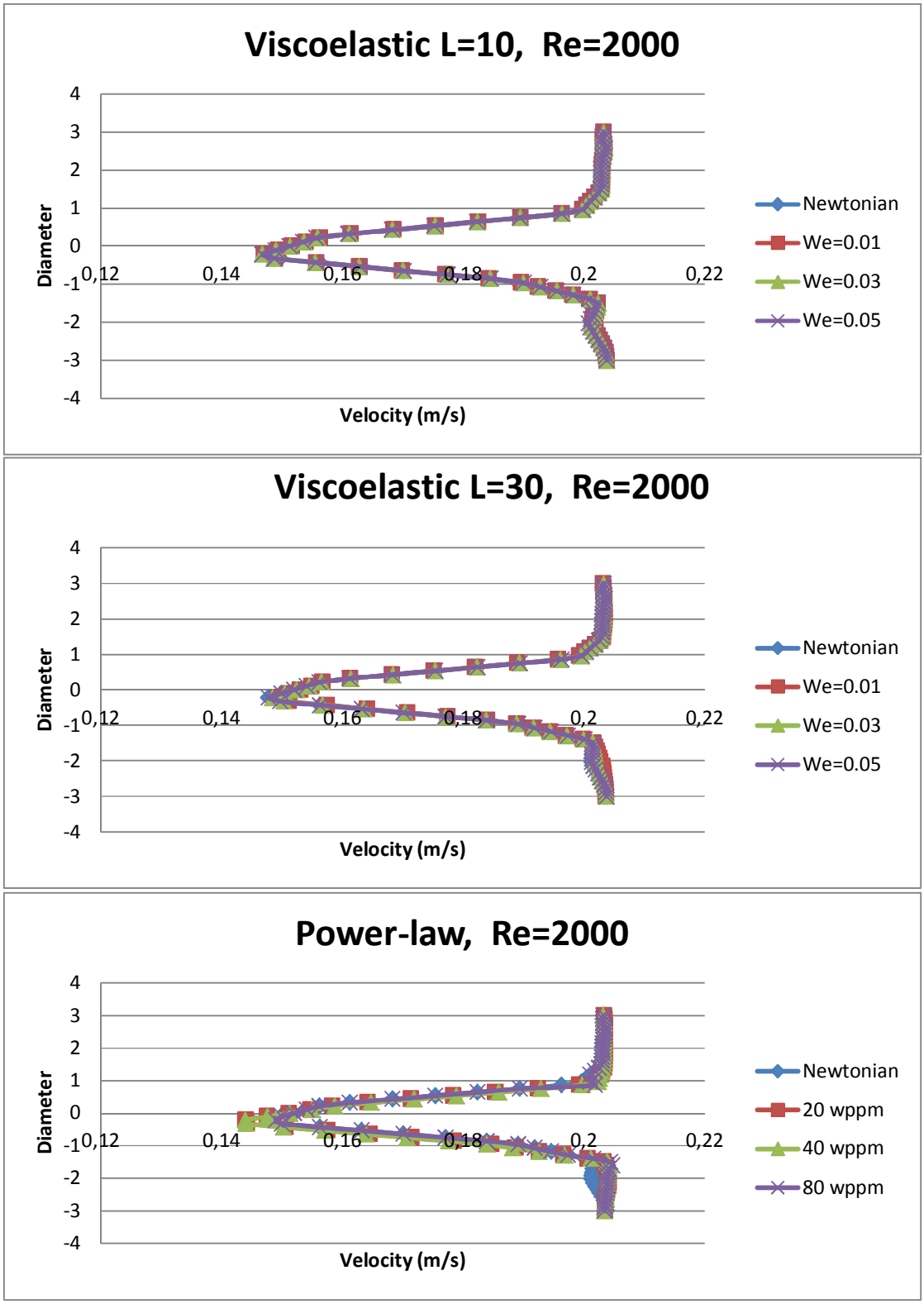

Figure 4.30. Circular cylinder wake region RMS velocity comparison for *Re* = 2000.

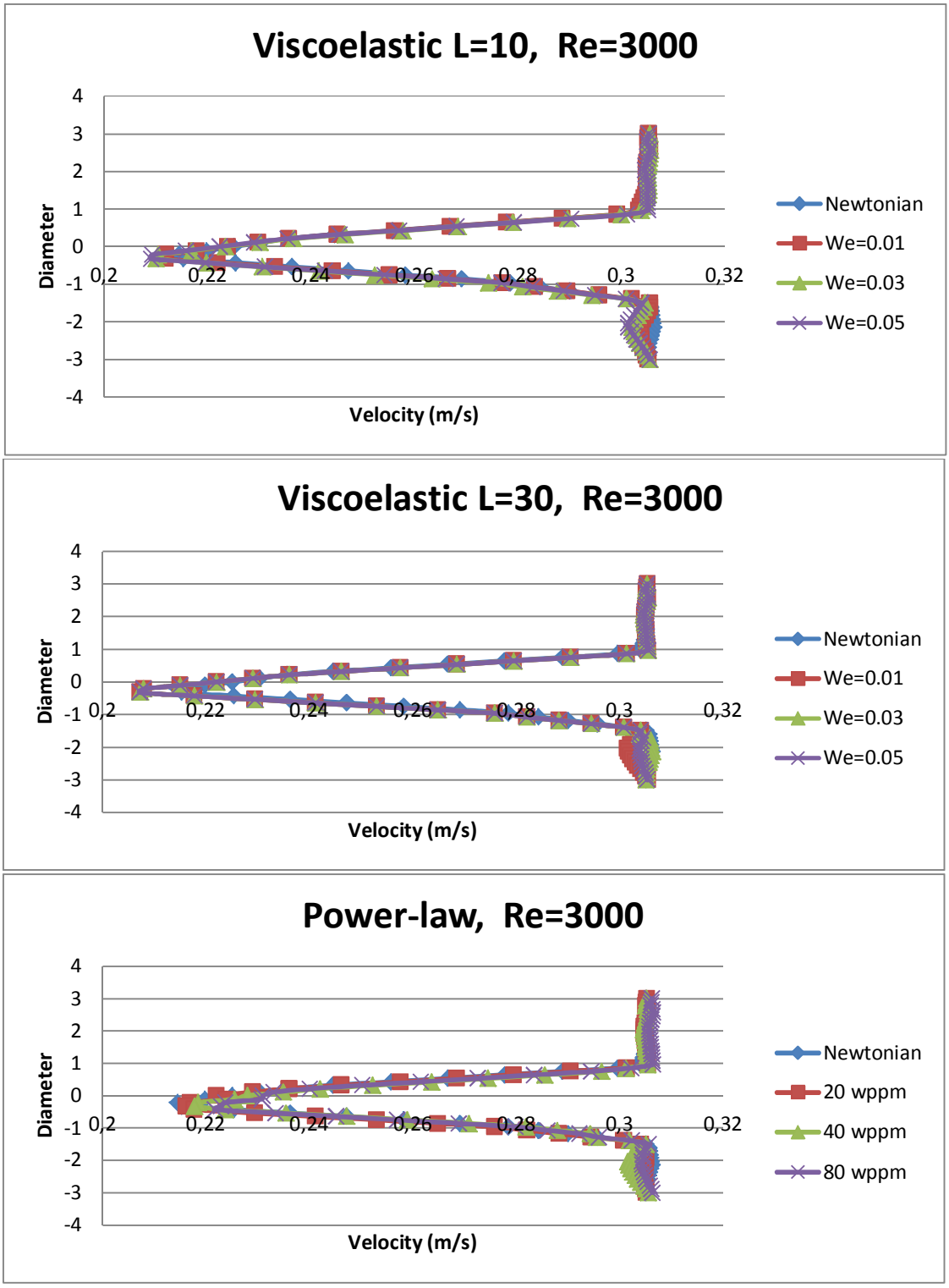

Figure 4.31. Circular cylinder wake region RMS velocity comparison for *Re* = 3000.

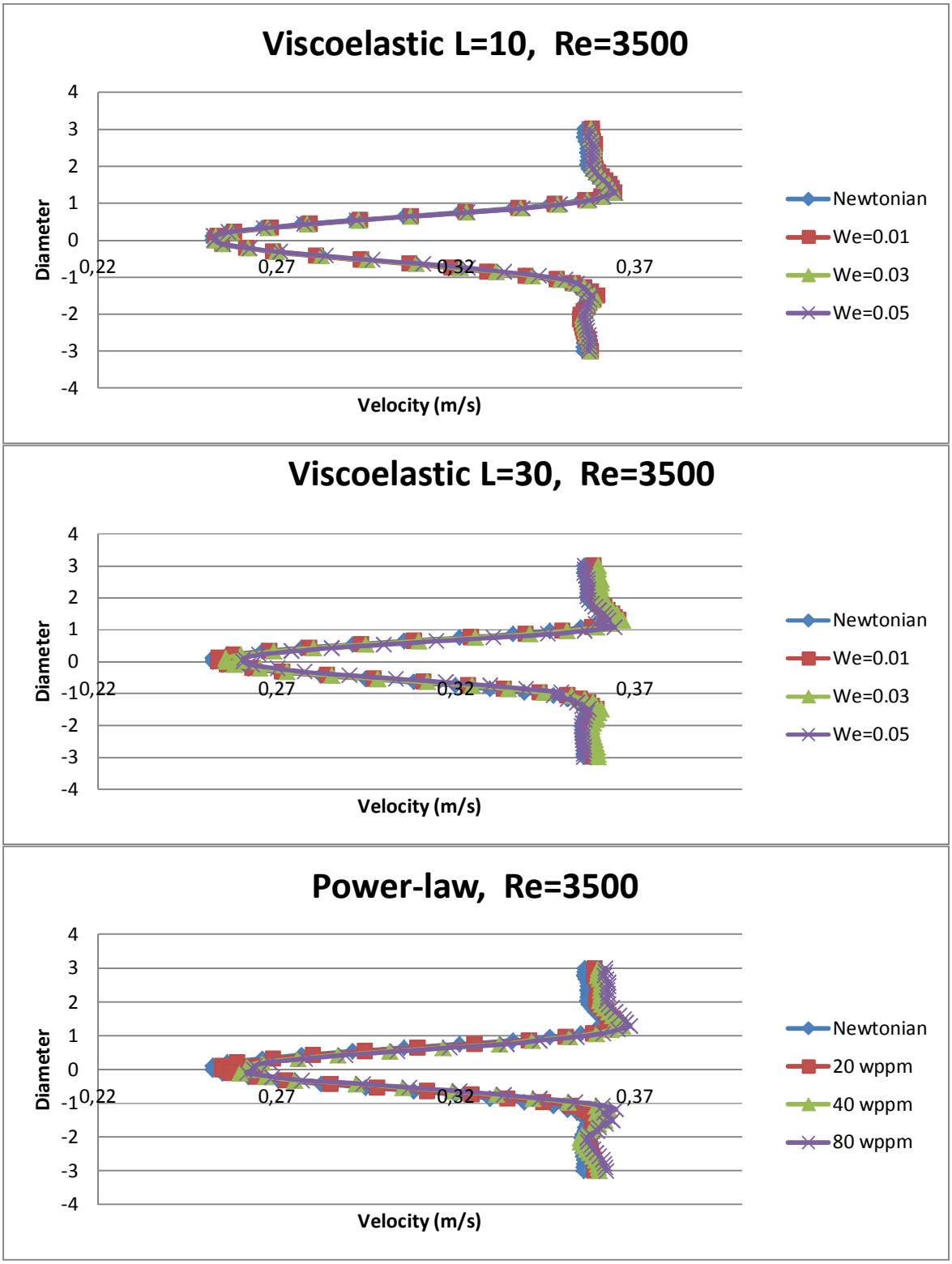

Figure 4.32. Circular cylinder wake region RMS velocity comparison for *Re* = 3500.

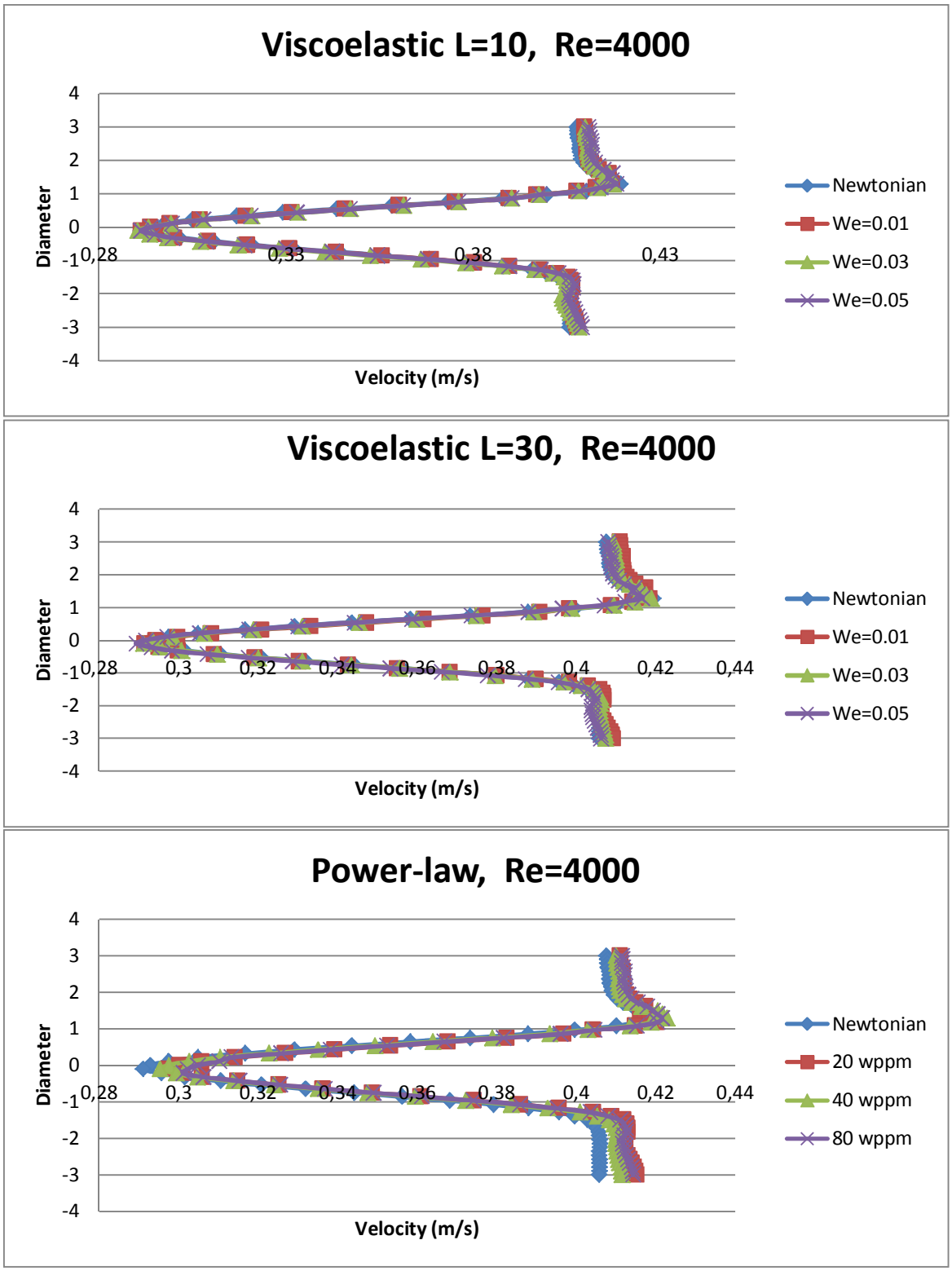

Figure 4.33. Circular cylinder wake region RMS velocity comparison for *Re* = 4000.

It can be observed that as Reynolds number increases, the wake region is getting narrower and the velocities in the wake region are getting smaller compared to the mean fluid velocity. The reason is that as the ratio of inertial forces to the viscous forces increases in a flow case, the effect of a blocking body decreases for the outside portion of the flow domain. But, there is no certain conclusion related to polymer addition, according to the wake region velocity distribution graphs due to lack of a trend, increasing or decreasing, in the simulations. In other words, wake region flow velocity profiles do not show a distinctive trend in polymer induced simulations, compared to Newtonian simulations.

4.3.2. Wake Region Velocity Distribution in Square Cylinder Problem

Square cylinder wake region root mean square velocity distribution for varying Reynolds numbers shown in Figures 4.35 - 4.38. Figure 4.34 shows an instantaneous velocity vector distribution for Newtonian fluid at Re = 1000.

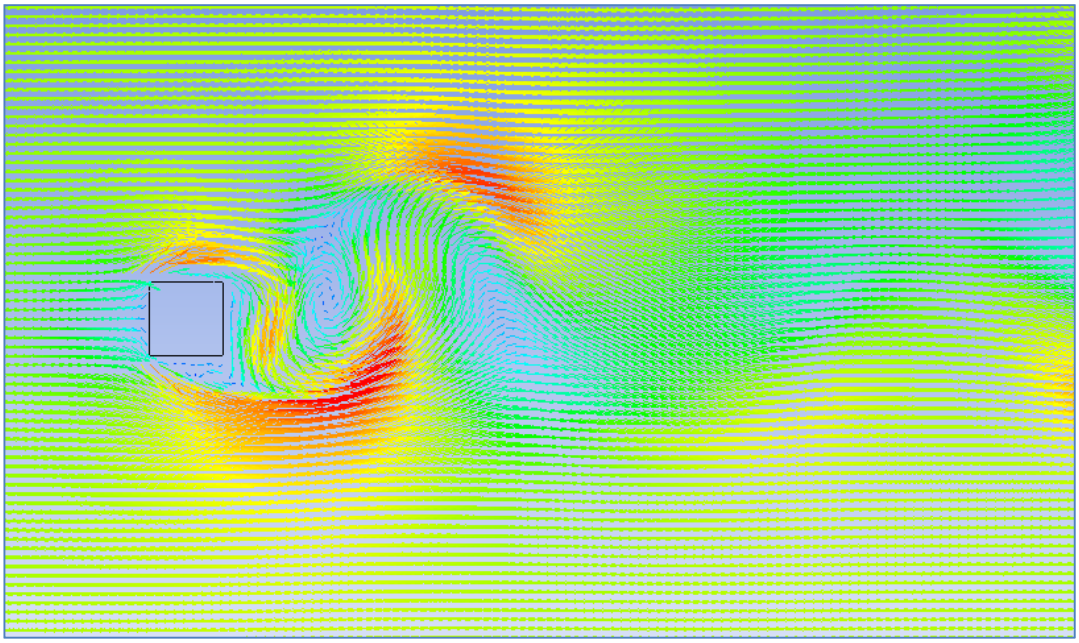

Figure 4.34. Instantaneous velocity vector distribution in squarer cylinder problem domain, (Newtonian fluid, Re = 1000).

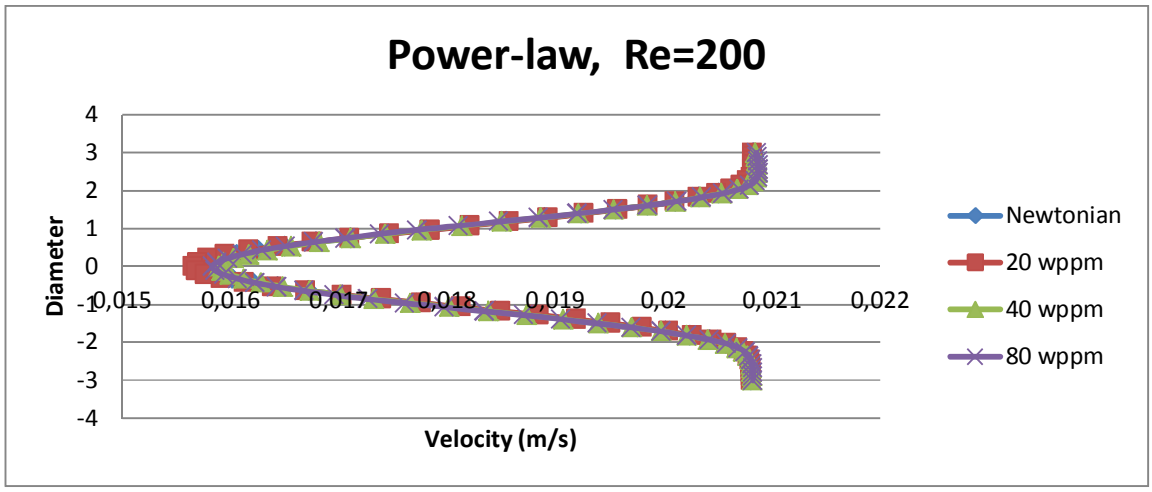

Figure 4.35. Square cylinder wake region RMS velocity comparison for *Re* = 200.

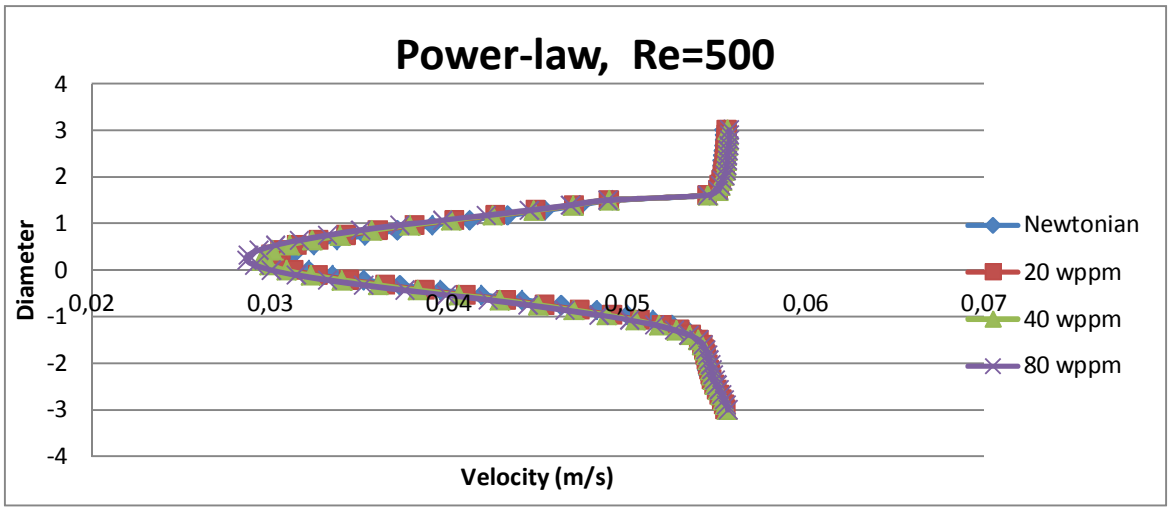

Figure 4.36. Square cylinder wake region RMS velocity comparison for *Re* = 500.

Square cylinder wake region velocity distribution results show that the wake region is getting narrower as Reynolds number increases. There is no clear sign related to polymer addition due to lack of a trend, neither increasing nor decreasing, according to the simulations.

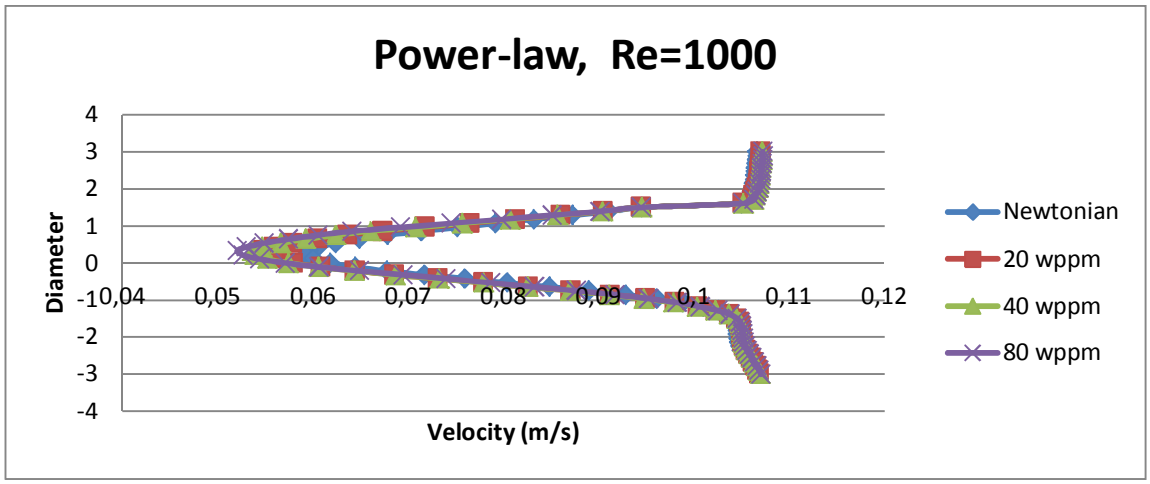

Figure 4.37. Square Cylinder Wake Region RMS Velocity Comparison for *Re* = 1000.

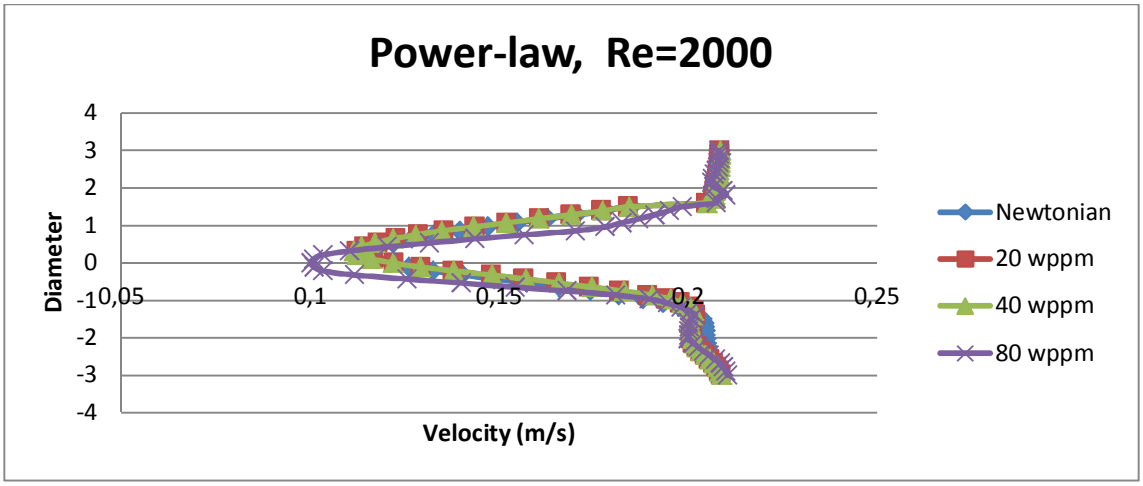

Figure 4.38. Square Cylinder Wake Region RMS Velocity Comparison for *Re* = 2000.

4.4. Strouhal Number

4.4.1. Strouhal Number Results in Circular Cylinder Problem

Trends of Strouhal number in circular cylinder simulations are given on Table 4.7 and Table 4.8 for varying Reynolds numbers for both viscoelastic (FENE-P model) and Power-law cases, compared to Newtonian results.

Table 4.7. Strouhal number trends for circular cylinder viscoelastic FENE-P simulations.

St	*Newtonian*	*We = 0.01 L = 10*	*We = 0.03 L = 10*	*We = 0.05 L = 10*	*We = 0.01 L = 30*	*We =0.03 L=30*	*We=0.05 L=30*
Re = 200	0.176	0.175	0.176	0.177	0.182	0.180	0.179
Re = 500	0.208	0.206	0.210	0.207	0.202	0.201	0.201
Re = 1000	0.233	0.233	0.229	0.242	0.237	0.246	0.238
Re = 2000	0.260	0.251	0.254	0.250	0.250	0.249	0.252
Re = 3000	0.252	0.261	0.257	0.254	0.265	0.255	0.254
Re = 3500	0.261	0.271	0.245	0.243	0.271	0.269	0.255
Re = 4000	0.231	0.223	0.239	0.245	0.237	0.246	0.238

Table 4.8. Strouhal number trend for circular cylinder Power-law simulations.

St	*Newtonian*	*20 wppm*	*40 wppm*	*80 wppm*
Re = 200	0.176	0.180	0.175	0.189
Re = 500	0.208	0.221	0.221	0.242
Re = 1000	0.233	0.270	0.256	0.255
Re = 2000	0.260	0.250	0.249	0.252
Re = 3000	0.252	0.263	0.27	0.28
Re = 3500	2.261	0.273	0.277	0.282
Re = 4000	0.231	0.226	0.236	0.249

As a result, it may be stated that there is no general trend seen on Strouhal Number, i.e. vortex formation frequency, with polymer addition for viscoelastic FENE-P model. However, an increasing trend with polymer addition for Strouhal number, in most of the cases, is observed in Power-law simulations. This result is in parallel with Coelho and Pinho's experimental study [16].

4.4.2. Strouhal Number Results in Square Cylinder Problem

Values of Strouhal number in square cylinder simulations, from *Re* = 200 to *Re* = 2000, are given in Table 4.9. The results are close to the experimental results of a recent study [46] due to the increasing trend with polymer addition.

Table 4.9. Strouhal number trend for square cylinder Power-law simulations.

St	*Newtonian*	*20 wppm*	*40 wppm*	*80 wppm*
Re = 200	0.141	0.140	0.147	0.152
Re = 500	0.133	0.133	0.138	0.139
Re = 1000	0.125	0.125	0.129	0.132
Re = 2000	0.130	0.133	0.132	0.135

5. CONCLUSIONS

The main objective of this thesis is the investigation of polymer additive effects on flow around circular and square cylinders; and understanding of the underlying mechanism of this effect. It has been evaluated by means of several flow parameters, such as drag coefficient, vortex formation length, wake region velocity distribution, vortex shedding frequency (Strouhal Number).

The main conclusions of the study can be itemized as;

- Drag coefficient shows a decreasing trend, with polymer addition, on circular cylinder Generalized Newtonian simulations (Power-law model). On the other hand, circular cylinder viscoelastic (FENE-P model) simulations show increase in drag coefficient for $200 < Re \leq 3000$, and decrease in drag coefficient for $3500 \leq Re \leq 4000$. Square cylinder simulations, which are performed with Power-law fluid for polymer addition modeling, show a similar conclusion with circular cylinder results, i.e. drag reduction with polymer addition. Therefore, it can be concluded that instabilities and anisotropy created by polymer addition are the result of drag reduction on turbulent flows, instead of viscoelastic effects composed of polymer addition. This conclusion is partially in parallel with den Toonder's studies [19, 20], which states that the reason for drag reduction by polymer additives is viscous anisotropic stresses introduced by extended polymer and that elasticity has an adverse effect on drag reduction.
- In circular cylinder Power-law model simulations, the vortex formation length parameter has a decreasing trend for $Re < 3000$ whereas it has an increasing trend for $Re \geq 3000$; and in circular cylinder viscoelastic (FENE-P model) simulations, there is a general trend of decreasing vortex formation length. In square cylinder Power-law model simulations, the vortex formation length has a decreasing trend for $Re < 2000$ whereas it has an increasing trend for $Re \geq 2000$. Hence, it can be conducted that vortex formation length decreases with polymer addition for Reynolds numbers smaller than 2000.

- In circular cylinder simulations, it is observed that there is mostly an increasing Strouhal number trend with polymer addition for Power-law model, in spite of lack of a general trend for FENE-P model. In square cylinder simulations, Strouhal number has an increasing trend with polymer addition. Therefore, it worth to conclude that the frequency of the wake region vortex generation increases by means of polymer additives. This conclusion is in parallel with Coelho and Pinho's [16]; whereas it opposes to a previous study by Kudin and Kalashnikov [12], who showed that vortex shedding frequency is smaller for polymer added flows compared to the Newtonian ones.
- The other significant conclusion in the study is the relation between drag coefficient and vortex formation length trends. At high Reynolds numbers, i.e. $Re \geq 3000$ in circular cylinder problem and $Re = 2000$ in square cylinder problem, vortex formation length shows an increasing trend with polymer addition on Power-law simulations of both circular and square cylinder domains, where the drag coefficient reduces with polymer addition. This consequence is in parallel with Xiong's study [20], which states the drag coefficient and vortex formation length have adverse effect on each other; however another study of him on flow around circular cylinders [21] shows that the drag coefficient reduces with increasing Weissenberg number, *We*, which indicates the polymer concentration in viscoelastic studies, and this is not an outcome of this thesis since there is no drag reduction trend on viscoelastic (FENE-P model) simulations.
- The circular cylinder Power-law model simulations are in parallel with a recent study by Son [42], with respect to vortex formation length parameter because in both Son's study and in this study, polymer addition results in vortex formation length increase for $Re < 3000$ as well as a vortex formation length decrease for $Re \geq 3000$.

Since water becomes a non-Newtonian fluid by polymer addition and non-Newtonian fluid mechanics is still an unclear part of fluid mechanics discipline, it is not so easy to put the polymer additive effects on flow around cylinders into a reliable basis. However, each study, theoretical or practical, develops the global knowledge about this subject. Thus, this work,

although it does not clarifies everything, puts a small milestone to help this development by giving some conclusive results that are in parallel with previous studies.

In order to develop the existing knowledge about the polymer additive effects on the flow around immersed bodies, investigation of both circular cylinder and square cylinder problems in a wider Reynolds number range, by means of different rheological constitutive models, could be useful. It is also needed to perform more detailed experimental studies, and the results of the experimental studies need to be compared with advanced constitutive models, which represent different drag reduction mechanisms.

REFERENCES

1. Zdravkovich, M. M., *Flow Around Circular Cylinders*, Oxford University Press, New York, Vol. 1, 1997.

2. Wahl, H. A., W. R. Beaty, J. G. Dopper and G. R. Hass, "Drag Reducer Increases Oil Pipeline Flow Rates", *Offshore South East Asia Conference*, Singapore, 1982.

3. Unthank, J. L., S. G. Lalka, J. C. Nixon and A. P. Sawchuk, "Drag Reducing Polymers Selectively Improve Blood Flow Through Arterial Stenoses", *FASEB Journal*, Vol. 6, pp. 1471, 1992.

4. Toms, B. A., "On the Early Experiments on Drag Reduction by Polymers", *Physics of Fluids*, Vol. 20, pp. 3-5, 1977.

5. Burger, E. D., W. R. Munk and H. A. Wahl, "Flow Increase in the Trans-Alaska Pipeline Through Use of a Polymeric Drag-Reducing Additive", *Journal of Petroleum Technology*, Vol. 34, pp. 2, 1982.

6. Fabula, A. G., J. H. Green and W. F. Madison, "Torpedo Drag Reduction Employing Polymer Ejection", U.S. Patent no. 4,186,679, 1980.

7. Sellin, R. H. J., "Application of Polymer Drag Reduction to Sewer Flow Problems", *AIAA Paper*, pp. 88-366, 1988.

8. Oldaker, D. K. and W. G. Tiederman, "Spatial Structure of the Viscous Sub-layer in Drag Reducing Channel Flows", *Physics of Fluids*, Vol. 20, pp. 133-S144, 1977.

9. Toms, B. A., "Some Observations on the Flow of Linear Polymer Solutions Through Straight Tubes at Large Reynolds Numbers", *International Congress on Rheolgy*, Vol. 1, pp. 135-141, 1949.

10. Mysels, K.J., “Flow of Thickened Fluids”, U.S. Patent no. 2,492,173, 1949.

11. Gadd, G. E., “Effects of Long-chain Molecule Additives in Water on Vortex Streets”, *Nature*, Vol. 211, pp. 169–170, 1966.

12. Kalashnikov, V.N. and A.M. Kudin, “Kármán Vortices in the Flow of Drag-reducing Polymer Solutions”, *Nature*, Vol. 225, pp. 445–446, 1970.

13. Sarpkaya, T., P. G. Rainey and R. E. Kell, “Flow of Dilute Polymer Solutions About Circular Cylinders”, *Journal of Fluid Mechanics*, Vol. 57, pp. 177–208, 1973.

14. Cadot, O. and S. Kumar, “Experimental Characterisation of Viscoelastic Effects on Two and Three Dimensional Shear Instabilities”, *Journal of Fluid Mechanics*, Vol. 416, pp. 151–172, 2000.

15. Oliveira, P.J., “Method for Time-dependent Simulations of Viscoelastic Flows: Vortex Shedding Behind Cylinder”, *Journal of Non-Newtonian Fluid Mechanics*, Vol. 101, pp. 113–137, 2001.

16. Coelho, P.M. and F.T. Pinho, “Vortex Shedding in Cylinder Flow of Shear-thinning Fluids Identification and Demarcation of Flow Regimes”, J*ournal of Non-Newtonian Fluid Mechanics*, Vol. 110, pp. 143–176, 2003.

17. De Gennes, P. G., *Introduction to Polymer Dynamics*, Cambridge University Press, 1990.

18. Lumley, J. L., “Drag Reduction by Additives”, *Annual Review Fluid Mechanics*, Vol. 1, pp. 367-384, 1969.

19. Den Toonder, J. M. J., M. A. Hulsen, G. D. C. Kuiken and F. T. M. Nieuwstadt, “Drag Reduction by Polymer Additives in a Turbulent Pipe Flow: Numerical and Laboratory Experiments”, *Journal of Fluid Mechanics*, Vol. 337, pp. 193–231, 1997.

20. Den Toonder, J. M. J., *Drag Reduction by Polymer Additives in a Turbulent Pipe Flow: Laboratory and Numerical Experiments*, Ph. D. Thesis, *Delft University of Technology*, 2005.

21. Dimitropoulos, C. D., R. Sureshkumar and A. N. Beris, "Direct Numerical Simulation of Viscoelastic Turbulent Channel Flow Exhibiting Drag Reduction: Effect of the Variation of Rheological Parameters", *Journal of Non-Newtonian Fluid Mechanics*, Vol. 79, pp. 433–468, 1998.

22. Ogata, S., Y. Osano and K. Watanabe, "Effect of Surfactant Solutions on the Drag and the Flow Pattern of a Circular Cylinder" *American Institute of Chemical Engineers Journal*, Vol. 52, pp. 49-57, 2006.

23. Xiong, Y.L. "Numerical Investigation on Drag Reduction and Two-dimensional Turbulence in Diluted Polymer Solutions", *Bordeaux Universite-1*, 2010.

24. Xiong, Y. L., C.H. Bruneau and H. Kellay, "Flow Past a Cylinder in Diluted Polymer Solutions", *Journal of Physics: Conference Series*, Vol. 318, 2011.

25. Bearman, P. W. and E. D. Obasaju, "An Experimental Study of Pressure Fluctuations on Fixed and Oscillating Square-section Cylinders, *Journal of Fluid Mechanics*, Vol. 119, pp. 297-321, 1982.

26. Durao, F. G., M. V. Heitor and J. C. F. Pereira, "Measurements of Turbulent and Periodic Flows Around a Square Cross-section Cylinder, *Experiments in Fluids*, Vol. 6, pp. 298-304, 1988.

27. Luo, S. C., Y. T. Chew and Y. T. Ng, "Hysteresis Phenomenon in the Galloping Oscillation of a Square Cylinder", *Journal of Fluids and Structures*, Vol. 18, pp.103-118, 2003.

28. Dutta, S., K. Muralidhar and P. K. Panigrahi, "Influence of the Orientation of a Square Cylinder on the Wake Properties", *Experiments in Fluids*, Vol. 34, pp.16–23, 2003.

29. Bird, R. B., R. C. Armstrong and O. Hassager, *Dynamics of Polymeric Liquids, Volume 1*, Wiley, Canada, 1987.

30. Munson, B. R., D. F. Young and T. H. Okiishi, *Fundamentals of Fluid Mechanics, Fifth Edition*, John Wiley and Sons, Inc., 2006.

31. Hollister, S. J., *Bio-solid Mechanics: Modeling and Applications Lectures Web Page,* http://www.engin.umich.edu/class/bme456/, Michigan Engineering 2013, accessed at December 2012.

32. Leal, L. G., "Dynamics of Dilute Polymer Solutions: Structure of Turbulence and Drag Reduction", *Springer IUTAM Symposium*, pp. 155-185, 1989.

33. *Newton's Resistance Law and Stokes's Law*, *Aerosol Science and Engineering Webpage* , http://www.aerosols.wustl.edu/, Washington University in St. Louis, 2013, accessed at December 2012.

34. Dimotakis, P., P. Diamond, F. Dyson, D. Hammer, J. Katz and D. Nelson, "Turbulent Boundary-Layer Drag Reduction", *Mitre Corporation*, pp. 17-36, 2003.

35. Peet, Y., P. Sagaut and Y. Charron, "Turbulent Drag Reduction Using Sinusoidal Riblets with Triangular Cross-Section", *AIAA Journal*, Vol. 38, pp. 37-45, 2008.

36. Paschkewitz, J. S., Y. Dubief, C. D. Dimitropoulos, E. S. G. Shaqfeh and P. Moin, "Numerical Simulation of Turbulent Drag Reduction Using Rigid Fibers", *Journal of Fluid Mechanics*, Vol. 518, pp. 281-317, 2004.

37. Bajor, G., "Birdlike Photos, Swirl Vortex", Flickr Website, http://www.flickr.com/, 2008, accessed at December 2012.

38. Westerweel, J. "Digital Particle Image Velocimetry - Theory and Application", *Delft University of Technology*, 1993.

39. Eggels, J. G. M., "Direct and Large Eddy Simulation of Turbulent Flow in a Cylindrical Pipe geometry", *Delft University of Technology*, 1994.

40. Çelik, İ. B., Introductory Turbulence Modeling Lecture Notes, *West Virginia University Mechanical and Aerospace Engineering Department*, 1999.

41. Ritcher, D., E. S. G. Shaqfeh and G. Iaccarino, "Numerical Simulation of Polymer Injection in Turbulent Flow Past a Circular Cylinder", *Journal of Fluids Engineering*, Vol. 133, 2011.

42. Sahu, A. K., R. P. Chhabra and V. Eswaran, "Two-dimensional Unsteady Laminar Flow of a Power-law Fluid Across a Square Cylinder", J*ournal of Non-Newtonian Fluid Mechanics*, Vol. 160, pp. 157-167, 2009.

43. Mercan, H., *Numerical Investigation of Isothermal and Non-Isothermal Viscoelastic Flow in Lid-driven Polar Cavity*, Ph. D. Thesis, *Boğazici University*, 2012.

44. Norberg, C., "Effects of Reynolds Number and a Low-intensity Freestream Turbulance on the Flow Around a Circular Cylinder", Department of Applied Thermodynamics and Fluid Mechanics, *Chalmers University of Technology*, Vol. 87, 1987.

45. Son, O., *Effects of Polymer Addition on Flow Properties and Structures Around Cicular Cylinders*, M. S. Thesis, *Istanbul Technical University*, 2010.

46. Wilkinson, B. and C. M. Allen, *Parallel Programming: Techniques and Applications Using Networked Workstations and Parallel Computers*, First Edition, Prentice Hall, Upper Saddle River, N.J., 1999.

47. Antonia, R. A. and S. Rajagopalan, "Determination of Drag of a Circular Cylinder", *AIAA Journal*, Vol. 28, pp. 1833-1834, 1990.

48. Schlichting, H., *Boundary-Layer Theory*, McGraw Hill Inc., 1979.

49. Atalik, K., O. Cetiner, O. Son, and O. Cetin, “Cisim Etrafi Akıslarda Polimer ve Sürfaktant Katkısının Yüksek Reynolds Sayılarında Akıs Özellikleri ve Yapısındaki Etkilerinin Deneysel ve Sayısal Olarak İncelenmesi”, *TUBITAK,* 107M390, 2010.